nature communications

Article

https://doi.org/10.1038/s41467-025-65996-2

Apoptosis-resistant cells drive compensatory proliferation via cell-autonomous and non-autonomous functions of the initiator caspase Dronc

Received: 10 December 2024

Accepted: 24 October 2025

Published online: 04 December 2025

Check for updates

Tslil Braun[1], Naama Afgin[1], Lena Sapozhnikov[1], Ehud Sivan[2], Andreas Bergmann[3], Luis Alberto Baena-Lopez[4], Keren Yacobi-Sharon[1] & Eli Arama[1]

Caspases are best known for promoting apoptosis, yet their role in tissue regeneration by compensatory proliferation remains unclear. Using *Drosophila* wing discs and a delayed reporter for the initiator caspase-9 ortholog Dronc activity, we identify two apoptosis-resistant epithelial cell populations that mediate regeneration after ionizing radiation: Dronc-activating (DARE) and non-activating (NARE) cells. Dronc activity in DARE cells, independent of Dark and effector caspases, drives regeneration both cell-autonomously and non-cell-autonomously. The TNFR in DARE cells, Wengen, likely activated by ROS, strongly promotes DARE proliferation, while TNF/Eiger and TNFR Grindelwald moderately suppress it. Downstream, p38 MAPK is the main signaling essential for DARE and NARE cell proliferation. Myo1D ensures DARE survival by preventing lethal effector caspase activation, whereas Myo7A/Crinkled supports moderate caspase activity. Dying cells trigger DARE induction, and both DARE and NARE transmit apoptosis resistance to progeny, with DARE progeny showing enhanced resistance. Maintaining balanced DARE-NARE proliferation is crucial for proper regeneration, growth, and differentiation, insights that may be relevant to radiation-resistant cells in cancer therapy.

Programmed cell death (PCD) is a genetically regulated process that eliminates unwanted or potentially dangerous cells during development and homeostasis in multicellular organisms[1–3]. Disruption of PCD is linked to various diseases, including cancer and neurodegenerative disorders[1,4–6]. Apoptosis, the most prevalent form of PCD during animal development, is characterized by a conserved sequence of morphological and cellular events[7,8]. Biochemically, apoptosis is marked by the activation of caspases, a unique family of cysteine proteases[9,10]. Caspases are crucial for both the signaling and execution of apoptosis, and their activation is tightly regulated by various activating and inhibitory proteins[10–14]. Synthesized as inactive pro-enzymes, caspases undergo a precisely controlled proteolytic cascade to become active and to activate each other[10,11,15–17]. Initiator caspases, such as caspase-9 (intrinsic pathway) and caspase-8 (extrinsic pathway), cleave and activate effector caspases like caspase-3 and caspase-7[18,19], which orchestrate cell death by cleaving numerous cellular proteins[20,21]. Inadvertent activation of caspases is prevented by inhibitory proteins such as the Inhibitor of Apoptosis proteins (IAPs), which bind to and inhibit caspases[22–25].

The *Drosophila* genome encodes seven caspases, with the initiator caspase-9 ortholog Dronc and the effector caspases 3 and 7 orthologs,

[1]Department of Molecular Genetics, Weizmann Institute of Science, Rehovot, Israel. [2]Department of Life Sciences Core Facilities, Weizmann Institute of Science, Rehovot, Israel. [3]Department of Molecular, Cell, and Cancer Biology, UMass Chan Medical School, Worcester, MA, USA. [4]Centro de Biología Molecular Severo Ochoa, CSIC, Madrid, Spain. e-mail: eli.arama@weizmann.ac.il

Drice and Dcp-1, mediating most apoptotic events during development and stress[26–30]. Dronc, similar to caspase-9, is activated on the apoptosome through binding to the *Drosophila* Apaf-1 related killer (Dark) adapter protein and subsequently activates Drice and Dcp-1[29,31–37]. In living cells, the major *Drosophila* IAP, Diap1, inhibits Dronc and the effector caspases[22,38–40]. During apoptosis, pro-apoptotic Reaper family proteins bind to Diap1, relieving its inhibition of caspases[22,25,41–43].

Despite their well-established role in apoptosis, numerous non-lethal caspase-dependent cellular processes (CDPs) have been identified across various tissues and organisms. While the molecular mechanisms governing apoptosis and caspase activation are well-understood, research into CDPs has progressed more slowly due to the complexities of studying these processes in specific cell types and tissues in vivo. Nevertheless, over the past two decades, CDPs have garnered significant attention due to their important biological and pathological implications[44–53].

Compensatory proliferation is a regenerative response to extensive cell death due to trauma. Although the involvement of caspases has been proposed, the molecular details remained unclear[54–57]. Early evidence of this phenomenon was observed in *Drosophila* wing imaginal discs (WIDs), which regenerate after high-dose ionizing radiation (IR), presumably by increasing the proliferation of surviving cells[58–60]. Despite this, identifying and tracking the cells responsible for this regeneration has been challenging, inevitably leading to confusion with other tissue regeneration mechanisms. One such mechanism, known as apoptosis-induced proliferation (AiP), has particularly complicated the understanding of compensatory proliferation[54,57,61–70]. AiP is a phenomenon in which apoptotic cells release mitogenic signals that promote the proliferation of neighboring cells. While AiP has been implicated in some physiological contexts, in WIDs it has predominantly been studied under non-physiological conditions that generate so-called 'undead' cells[55]. These cells are induced to undergo apoptosis through pro-apoptotic gene overexpression or irradiation, but are kept alive by the ectopic expression of the baculovirus P35 protein, a specific effector caspase inhibitor. In this state, 'undead' cells activate Dronc but fail to undergo apoptosis, continuously secreting mitogenic signals that drive hyperproliferation and overgrowth of adjacent wild-type (WT) cells[61,63–65]. This led to the hypothesis that AiP might mediate compensatory proliferation via non-cell autonomous signals from dying cells[42,60,71,72]. However, since AiP in the WID has primarily been studied as a non-physiological phenomenon, and given that compensatory proliferation persists even when key AiP-associated signals such as Wingless/Wnt and Dpp/BMP are disrupted[73], it is likely that AiP and compensatory proliferation represent separate phenomena[54].

Here, we show that compensatory growth of the WID after IR is mediated by the balanced proliferation of two cell populations: one that activates Dronc, referred to as DARE cells (Dronc-activating radiation-induced apoptosis-resistant epithelial cells), and another that does not activate Dronc, termed NARE cells (non-Dronc-activating radiation-induced apoptosis-resistant epithelial cells). Tracking DARE cell lineage reveals that the majority of cells appear at ~24 h post-irradiation (hpi) and undergo extensive proliferation over the subsequent 24 h, leading to tissue regeneration. Re-irradiation of both DARE- and NARE-derived progeny results in significantly fewer dying cells, with the effect being much stronger in DARE progeny, together indicating a molecular memory of the resistance trait. Ablation of DARE cells, or DARE-specific downregulation of Dronc or p38 signaling, markedly reduces the proliferation of both DARE and NARE cells, thereby impairing tissue regeneration and resulting in a smaller WID size at 48 hpi. In contrast, inactivation of the apoptosome adapter Dark or the effector caspases in DARE cells has no detectable effect on the regeneration of this tissue. Interestingly, when the same genetic manipulations are applied to the entire posterior region of the WID, cell death is blocked and DARE cell induction is significantly reduced, suggesting that dying cells release signals that promote DARE cell induction. Consistent with the apoptosis-resistant nature of DARE cells, we show that Myo1D in these cells, known to localize Dronc to the basal cell membrane during AiP[68,69], suppresses effector caspase activation and thereby prevents DARE cell death. This reveals at least one mechanism that hinders effector caspase activation to ensure the survival of these cells despite the presence of active Dronc. In contrast, Myo7A/Crinkled, another unconventional myosin shown to interact with Dronc in non-apoptotic contexts[74], promotes moderate effector caspase activation, which may partly explain why not all DARE cells survive. We further provide evidence that the two Tumor Necrosis Factor (TNF) receptors, Grindelwald (Grnd) and Wengen (Wgn), exert antagonistic roles in DARE cells. Grnd, together with paracrine TNF (Eiger) likely secreted by NARE cells, modestly inhibits DARE cell proliferation, whereas Wgn, presumably activated by ROS produced within DARE cells, strongly promotes their proliferation. Downstream, we find both p38 and c-Jun N-terminal kinase (JNK) signaling in DARE cells to promote DARE cell proliferation, while p38 is more prominent in this matter and is also important non-cell autonomously to coordinate the proliferation of NARE cells. Finally, we demonstrate that the interplay between DARE and NARE cells maintains proliferative homeostasis, which is essential for tissue regeneration and proper organ growth and differentiation. Given the widespread clinical use of ionizing radiation in cancer therapy, these findings may have important implications for understanding treatment-resistant cells and the mechanisms driving cancer recurrence.

Results

Two related genetic reporters of Dronc activity show distinct biases toward dying or surviving irradiated epithelial cells

To explore the mechanisms behind compensatory proliferation in the *Drosophila* wing imaginal disc (WID), we first established a timeline of major tissue regeneration by monitoring apoptotic cell counts and changes in tissue area at various time points following exposure to 20 Gy of X-radiation. As outlined in Supplementary Fig. 1a, irradiation was performed on a mixed-stage larval population, and WIDs were subsequently dissected and analyzed from larvae that reached the wandering 3rd instar stage at 4, 24, and 48 h post-irradiation (hpi). Therefore, a larva analyzed at 48 hpi was irradiated nearly two days earlier in developmental time than one analyzed at 4 hpi, yet all were examined at the same wandering 3rd instar stage. Although these time points do not constitute a continuous time series, they were chosen to represent distinct phases of the regenerative process: initiation of apoptosis at approximately 4 hpi, peak accumulation of dying cells and reduction in WID size at 24 hpi, and a recovery phase at 48 hpi, when apoptotic cells are largely cleared and tissue size has normalized. Apoptotic cells were identified through immunostaining with the anti-cleaved Dcp-1 antibody, which specifically detects the cleaved/activated forms of the effector caspases Drice and Dcp-1[29] (jointly referred to as cDcp-1). As previously reported[29,75], numerous apoptotic cells are detectable as early as 4 hpi compared to non-irradiated (Non-irrad) WIDs, with a marked increase observed by 24 hpi (Fig. 1a, b). Consequently, measurements of the total WID area showed a significant reduction in size at both 4 and 24 hpi (Fig. 1a, c). At 48 hpi, the number of apoptotic cells decreases dramatically, and the WID area returns to normal size (Fig. 1a–c). These findings suggest that most cell death in the irradiated WID occurs within the first ~24 hpi, while extensive tissue regeneration, likely driven by the compensatory proliferation of apoptosis-resistant cells, predominantly takes place during the subsequent ~24 h. It is important to note that the lack of significant changes in the sizes of the WIDs between 4 and 24 hpi suggests that compensatory proliferation may start as early as 4 hpi, with the most pronounced effect occurring between approximately 24–48 hpi.

We next sought a specific marker to label the apoptosis-resistant cells that drive the regeneration of the WID. To achieve this, we examined a genetic reporter sensor for the activity of the initiator

https://doi.org/10.1038/s41467-025-65996-2

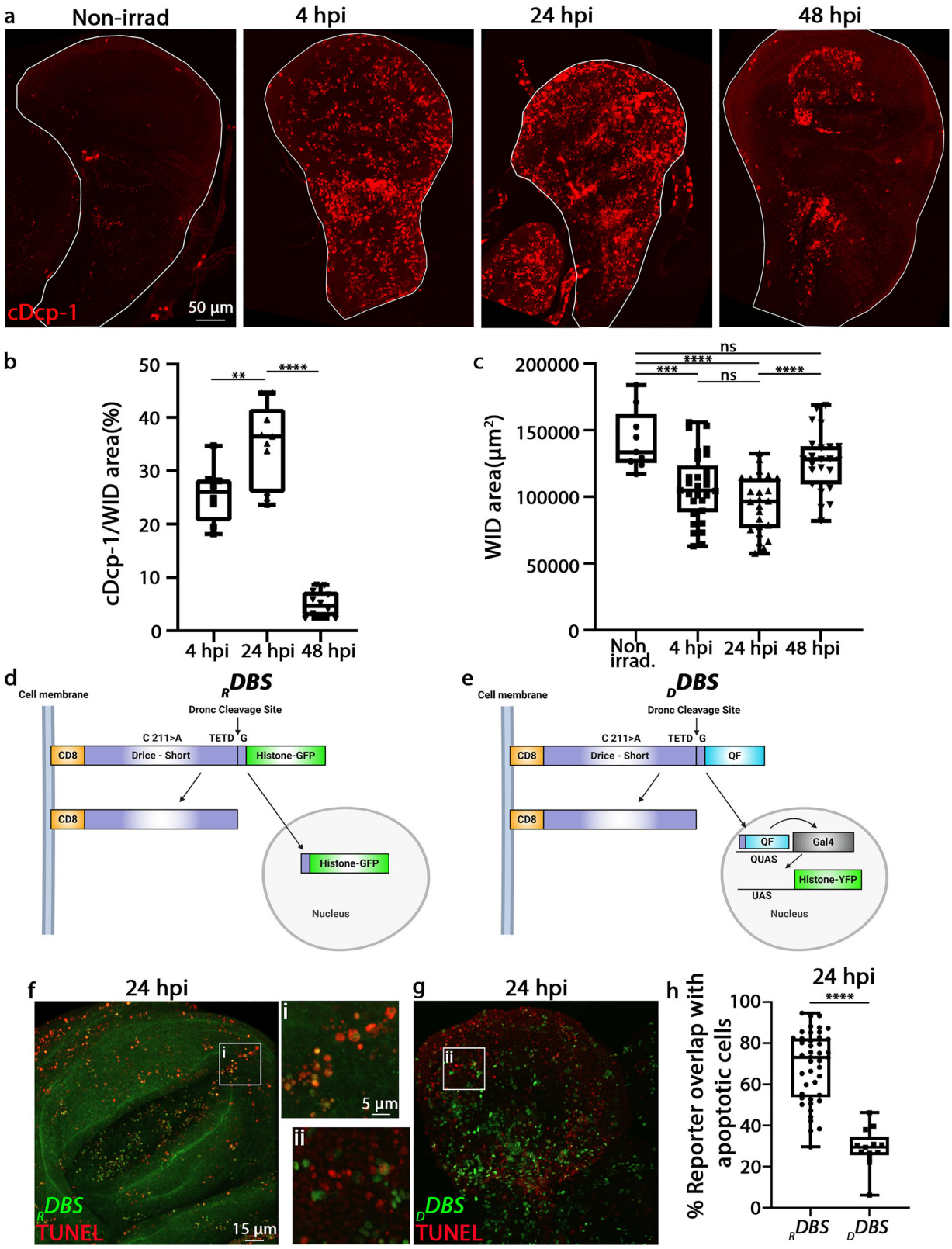

caspase Dronc. Beyond its role in initiating apoptosis by cleaving and activating effector caspases, Dronc has also been reported to mediate non-apoptotic cellular processes, including AiP[38,63,65,76,77]. We hypothesized that a delayed-reporting sensor of Dronc activity, relying on transcription and translation, would more specifically label surviving cells following ionizing radiation (IR). This hypothesis was based on the idea that apoptosis is typically associated with broad downregulation of basal transcription[78,79] and global inhibition of cap-dependent translation[80–83]. In contrast, rapid-reporting sensors that rely solely on mechanisms such as subcellular translocation primarily detect apoptotic cells, potentially overshadowing the identification of surviving cells. Therefore, a Dronc activity reporter that involves transcription/translation would likely preferentially label surviving cells, which are not subject to this inhibition. To investigate this hypothesis, we

Fig. 1 | Detection of irradiation-induced apoptosis-resistant cells using a delayed reporter of Dronc activity. a Representative WIDs from irradiated (20 Gy; X-rays) 3rd instar WT larvae immunostained to visualize dying apoptotic cells (cDcp-1; red). **b** Quantification of cell death in WIDs represented in (**a**) is expressed as the percentage of the WID area occupied by dying cells. **c** The graph depicts total size in square micrometers of the WIDs shown in (**a**). **d**, **e** Schematic representations of the Dronc activity genetic reporters *$_R$DBS* and *$_D$DBS* are shown before (upper) and after (lower) cleavage by Dronc. Created in BioRender. Braun, T. & Yacobi-Sharon, K. (2025) https://BioRender.com/s6ebqxl. **f**, **g** Irradiated WIDs expressing the *$_R$DBS* (**f**, green) or the *$_D$DBS* (**g**, green) were co-stained with TUNEL to detect dying cells (red). White boxes show magnifications of the outlined areas. **h** Quantification of co-labeling in the experiments shown in (**f**, **g**). Statistical tests: One-way ANOVA followed by Tukey's multiple comparisons test (**b**, **c**); two-tailed unpaired Student's *t*-test (**h**). All data points, including outliers, are displayed as box plots, with each point representing a single WID. Lower and upper whiskers represent the minimum and maximum values, respectively; the center line denotes the median; and the lower and upper box bounds correspond to the medians of the lower and upper halves of the dataset. Numbers (n) of WIDs examined were: 8 (4 hpi), 11 (24 hpi), and 12 (48 hpi) in (**b**); 9 (non-irradiated), 29 (4 hpi), 25 (24 hpi), and 23 (48 hpi) in (**c**); and 44 (*$_R$DBS*) and 13 (*$_D$DBS*) in (**h**) $^{**}p < 0.01$; $^{***}p < 0.001$; $^{****}p < 0.0001$; ns, not significant. *p*-values in (**b**): $p = 0.0021$ (4 hpi vs. 24 hpi), and $p < 0.0001$ (24 hpi vs. 48 hpi); (**c**): $p = 0.0007$ (non-irradiated vs. 4 hpi), $p = 0.2483$ (4 hpi vs. 24 hpi), $p < 0.0001$ (24 hpi vs. 48 hpi), $p < 0.0001$ (non-irradiated vs. 24 hpi), and $p = 0.3309$ (non-irradiated vs. 48 hpi); **h**: $p < 0.0001$ (*$_R$DBS* vs. *$_D$DBS*).

examined two related *Drice-based sensors* of Dronc activity: a rapid reporter sensor (*$_R$DBS*) and a delayed reporter sensor (*$_D$DBS*). While both have been previously described, *$_D$DBS* has been much less characterized than *$_R$DBS*[84]. These genetic reporters consist of two key components: a common N-terminal Dronc recognition element and two distinct C-terminal reporting elements (Fig. 1d, e). The Dronc recognition element consists of a C-terminally truncated, inactive form of the effector caspase-3 ortholog Drice, fused to an N-terminal mouse CD8 transmembrane domain. The reporting elements, fused to the C-terminus of the Dronc recognition element, consist of either a Histone H2B fused to GFP (Histone-GFP; in the *$_R$DBS*) or a QF transcription factor from the binary Q-system (*$_D$DBS*). Upon cleavage by Dronc, the reporting elements translocate from the cell membrane to the nucleus. In cells expressing the *$_R$DBS*, this movement is quickly detectable due to the chromatin being fluorescently labeled with GFP. In contrast, in our setup, detecting *$_D$DBS* sensor cleavage requires the presence of *QUAS*-dependent fluorescent proteins or *QUAS-Gal4* and *UAS*-dependent fluorescent protein constructs. The latter setup generates a fluorescent signal only after two sequential rounds of transcription and translation, first to produce Gal4, and subsequently to express the fluorescent protein (or any other protein of interest).

To investigate the behavior of the *$_D$DBS* reporter, we first examined WIDs from irradiated larvae (20 Gy X-rays) ubiquitously expressing the rapid reporter *$_R$DBS*. Consistent with the notion that this reporter rapidly detects Dronc activity in apoptotic cells, we found that, on average, 70% of the cells exhibiting nuclear Histone-GFP were TUNEL-positive at 24 hpi, confirming their apoptotic status (Fig. 1f, h). Since initiator caspase activation precedes TUNEL labeling of DNA fragmentation during apoptosis, we attribute the remaining 30% of Histone-GFP-positive cells to those in earlier stages of apoptosis. In stark contrast, irradiated WIDs expressing the *$_D$DBS* reporter, together with the *QUAS-Gal4* adapter and a *UAS-Histone-YFP* transgene (Histone H2B fused to YFP), showed that only about 30% of the nuclear YFP-positive cells (indicative of cleaved *$_D$DBS*) were also TUNEL-positive at 24 hpi (Fig. 1g, h). This suggests that the majority of cells detected by the *$_D$DBS* reporter are not undergoing apoptosis, but instead remain viable for at least 24 hpi despite exhibiting Dronc activation.

The *$_D$DBS* reporter labels epithelial cells that are resistant to irradiation-induced apoptosis

We next asked whether the cleaved *$_D$DBS*-positive cells represent apoptosis-resistant survivors or cells undergoing a delayed but ultimately inevitable apoptotic fate. To investigate this, we monitored both the *$_D$DBS* reporter and apoptotic cells at the various time points following irradiation. Specifically, we immunostained irradiated WIDs expressing the *$_D$DBS* reporter, together with *QUAS-Gal4* and *UAS-Venus* transgenic constructs (Fig. 2a), to simultaneously detect apoptotic cells marked by cDcp-1 and cleaved *$_D$DBS*-positive cells labeled with the yellow fluorescent protein Venus. In non-irradiated WIDs, we observed only a few cDcp-1-positive dying cells, as expected, and only a few Venus-positive small cell clones, with the two populations being largely mutually exclusive (Fig. 2bi). The observation that Venus-positive cells appeared as small clones suggests that, rather than undergoing apoptosis, some cells activate Dronc, survive, and undergo a few rounds of division, potentially compensating for the loss of developmentally dying cells. At 4 hpi, we observed a dramatic increase in the number of apoptotic cells (see also Fig. 1a), but only a modest rise in the number of cleaved *$_D$DBS*-positive cells and clones (Fig. 2bii, v, vi). At 24 hpi, there was a marked increase in the number of cleaved *$_D$DBS*-positive cells and clones, most of which showed no cDcp-1 expression (Fig. 2biii, vii, viii). This suggests that the *$_D$DBS* is more effective at detecting surviving cells that have activated Dronc, rather than the dying cells. Furthermore, by 48 hpi, both the number and size of *$_D$DBS*-positive cell clones had increased, with most of these clones being cDcp-1-negative (Fig. 2biv). This suggests that not all irradiated cells that activate Dronc undergo apoptosis; some of these cells survive, divide, and persist throughout the WID, even two days after irradiation. Note that as the clones grow in size and the fluorescent protein dilutes with each cell division, they become dim, making accurate quantification challenging, a technical limitation addressed in the next paragraph and subsequent experiments. Finally, this phenomenon is not limited to WIDs; *$_D$DBS*-positive cell clones were also observed in irradiated halteres, legs, and eye-antenna imaginal discs at 48 hpi (Fig. 2c). Notably, in the eye-antenna imaginal disc, this phenomenon was largely confined to the antennal region, with only a few DARE cells detected in the eye region. This observation aligns with the fact that, at this stage, the eye region is already undergoing photoreceptor specification and differentiation[85], which is also consistent with the distinct mechanisms governing AiP in the eye and antenna domains of the imaginal disc[64]. Collectively, these results reveal a natural population of radiation-induced Dronc-activating apoptosis-resistant epithelial (DARE) cells scattered throughout imaginal disc tissues. These cells increase in number 24 h after irradiation and are identified using a delayed genetic reporter of Dronc activity.

DARE cells extensively proliferate between 24–48 hpi and regenerate the WID

To overcome the technical challenge of DARE cell clones appearing dim at 48 hpi, due to dilution of the fluorescent protein with each cell division, we combined the *$_D$DBS* reporter system with a genetic cell lineage tracing system known as G-TRACE[86]. This system enables tracking of dividing cell lineages while preventing dilution of the fluorescent protein in their daughter cells (Fig. 3a)[86]. The G-TRACE system consists of three transgenic constructs: a *UAS-nRFP* for real-time red fluorescence, a *UAS-FLP* for Flippase expression, and a *FRT-stop-FRT-nEGFP* cassette for cell lineage tracing with green fluorescence. Combining the *$_D$DBS* reporter with the G-TRACE system ensures that, after three rounds of transcription and translation, DARE cells exhibit strong red or yellow (red plus green) fluorescence. In contrast, as DARE cells divide, their progeny cells should maintain constant green fluorescence intensity while showing a gradual decrease in red fluorescence with each cell division (Fig. 3a).

Consistent with our observation that tissue regeneration in irradiated WIDs predominantly occurs between ~24–48 hpi (Fig. 1c),

https://doi.org/10.1038/s41467-025-65996-2

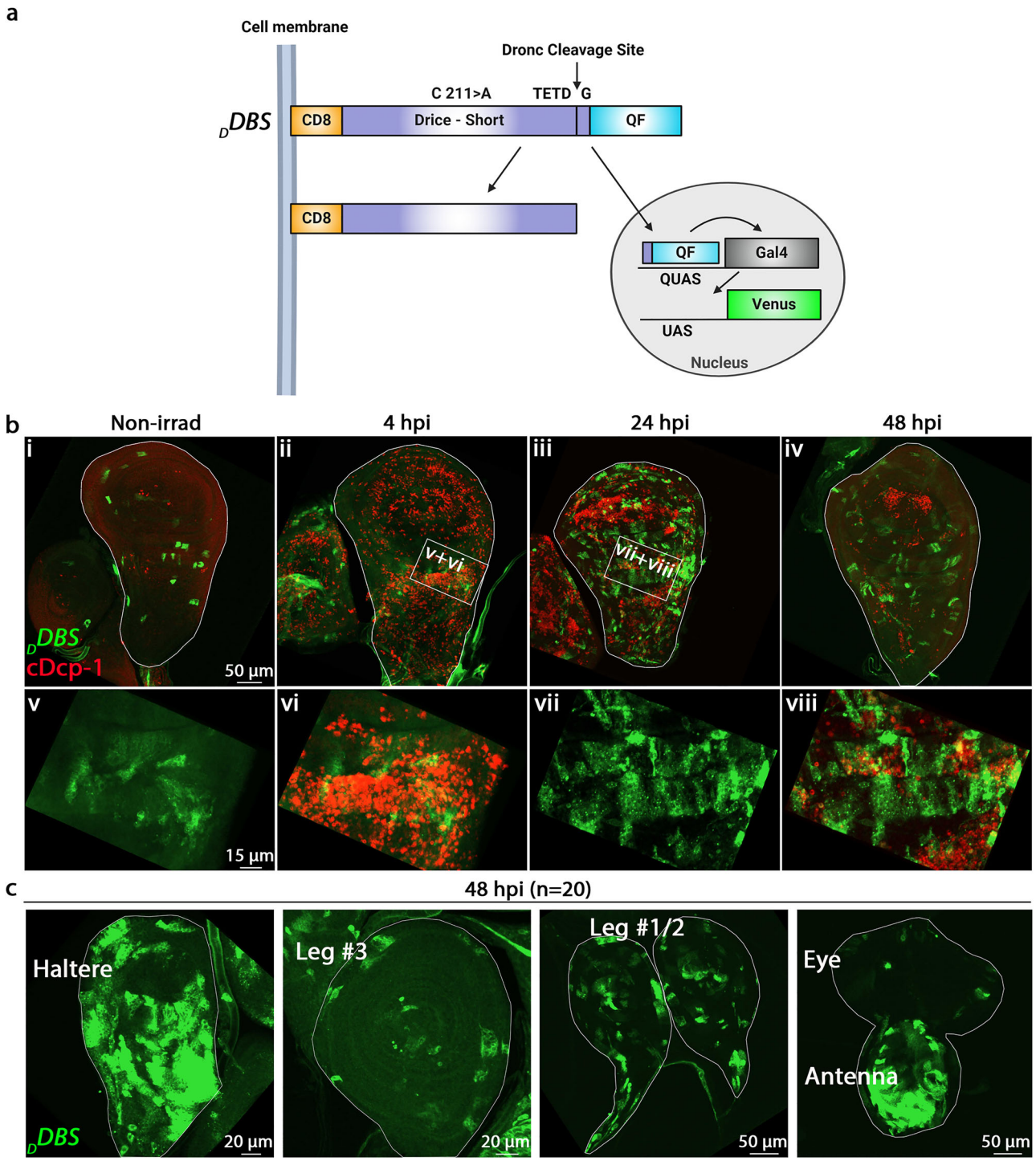

Fig. 2 | The *DBS* reporter primarily labels apoptosis-resistant cells surviving even 48 hpi. a Schematic representation of the *DBS* reporter combined with a *UAS-Venus* transgene. Created in BioRender. Braun, T. & Yacobi-Sharon, K. (2025) https://BioRender.com/s6ebqxl. **b** Irradiated WIDs expressing the transgenic combination described in (**a**) and immunostained to visualize dying apoptotic cells (cDcp-1; red). The images show representative WIDs before and at the indicated time points after irradiation displaying largely mutually exclusive expressions of active *DBS* (Venus; green) and cDcp-1 at 4 and 24 hpi, the periods of massive cell death. The outlined areas (white rectangles) are magnified in the row below. **c** Representative images of 48 hpi imaginal discs of the indicated types, expressing the transgenic combination described in (**a**). Cells that activated the reporter (Venus; green) are readily detected, occupying large areas of the tissues. $n = 20$ for each imaginal disc type.

only a few red and yellow cells, along with small green cell clones, are detected before irradiation and at 4 hpi, covering, on average, about 10% of the WID (Fig. 3bi, ii, c). Note that quantification of the area occupied by DARE cells and derived clones shows a modest but significant increase between non-irradiated and 4 hpi WIDs, supporting the idea that compensatory proliferation begins shortly after radiation-sensitive cells start dying (Fig. 3d). By 24 hpi, there is a significant increase in the number of DARE cells and derived clones, which are dispersed throughout the WID and collectively occupy approximately 30% of the tissue area on average (Fig. 3biii, c). Critically, by 48 hpi, both the number and size of DARE cell clones increase substantially, covering nearly 50% of the WID area on

https://doi.org/10.1038/s41467-025-65996-2

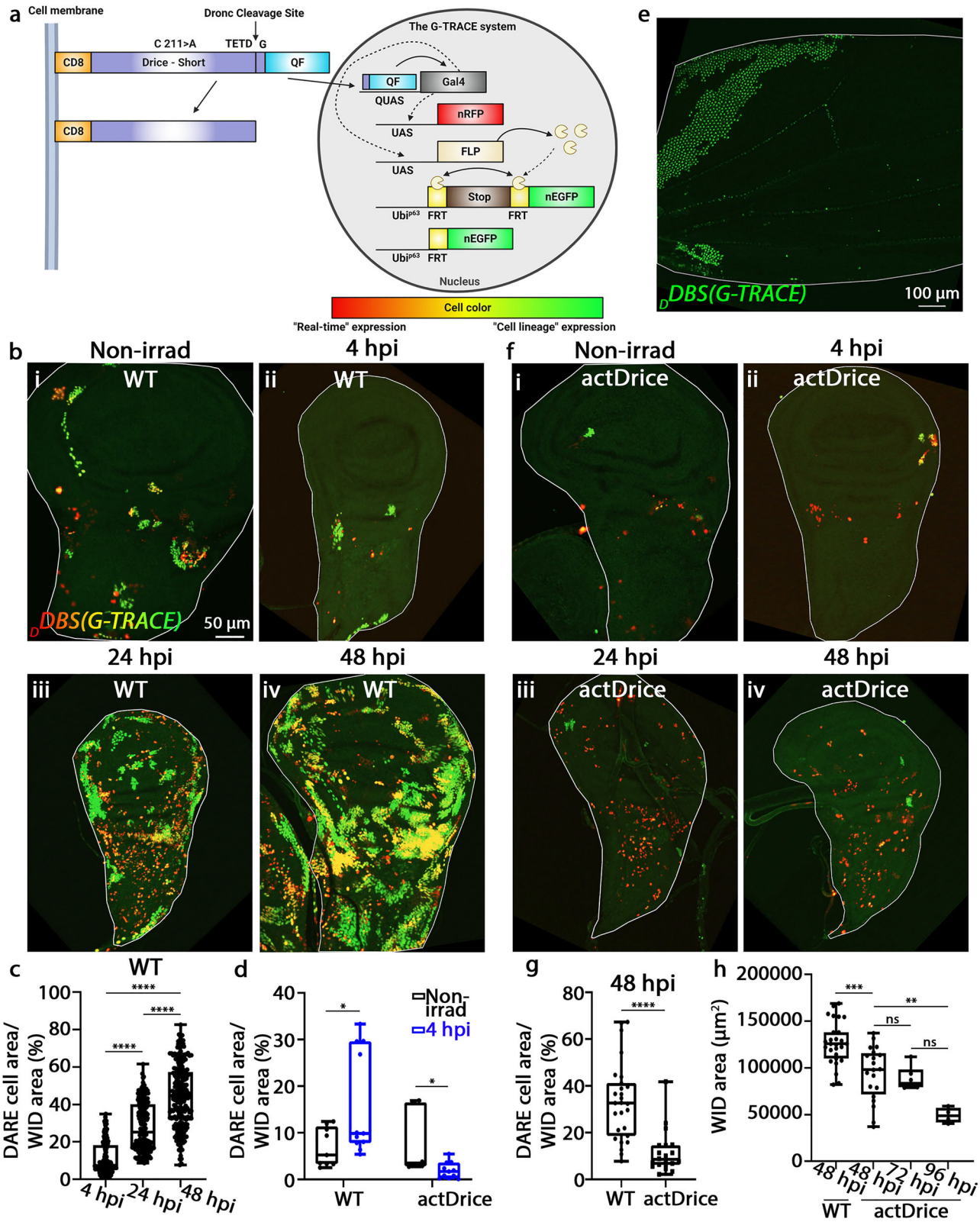

average, with some WIDs exhibiting over 80% coverage (Fig. 3biv, c). This suggests extensive proliferation of DARE cells between 24 and 48 hpi. Notably, the fluorescent cells observed are exclusively DARE cells and their derivative clones, as no fluorescence leakage is detected at any time point in irradiated WIDs containing the G-TRACE system but lacking the *DBS* reporter (Supplementary Fig. 1b).

During larval stages, the WID epithelium undergoes extensive patterning and growth. As the larvae enter pupation, the WIDs begin morphogenesis, during which epithelial cells delaminate, change shape, and secrete materials that contribute to the formation of the cuticle and mature wing structures[87,88]. Shortly after eclosion, the entire *Drosophila* wing epithelium undergoes rapid and synchronized apoptosis, with cells collectively eliminated through a 'suicide wave',

Fig. 3 | Multiple DARE cells predominantly appear at 24 hpi and extensively proliferate over the following 24 h to regenerate the WID. a Schematic of the *$_D$DBS* reporter combined with the G-TRACE system. Created in BioRender. Braun, T. & Yacobi-Sharon, K. (2025) https://BioRender.com/s6ebqxl. **b** WIDs expressing the transgenic combination described in (**a**) and monitored at the indicated time points after irradiation. **c**, **d** Quantification of total DARE cell fluorescent area shown in **biii-iv** (**c**) and **bi, ii and fi, ii** (**d**) expressed as a percentage of total WID area. **e** Adult wing shortly after eclosion derived from a 48 hpi larva (as in **biv**) displaying residual DARE cells (green). **f** Irradiated WIDs, as in (**b**), expressing the *actDrice* transgene in the DARE cells. **g** Quantification of total DARE cell fluorescent area shown in **biv** and **fiv** expressed as a percentage of total WID area. **h** Quantification of the total WID sizes (in square micrometers) in 48 hpi WT (**biv**) and *actDrice*-expressing DARE cells at 48 (**fiv**), 72, and 96 hpi. Statistical tests: One-way ANOVA followed by Tukey's multiple comparisons test (**c**, **h**); two-tailed unpaired Student's *t*-test (**d**, **g**). All data points, including outliers, are shown in box plot format. The lower and upper whiskers represent the minimum and maximum values, respectively; the center line denotes the median; and the lower and upper box bounds correspond to the medians of the lower and upper halves of the dataset. Each dot represents a single WID, reflecting the number of biologically independent WID samples (n). Numbers (n) of WIDs examined were: 202 (4 hpi), 178 (24 hpi), and 224 (48 hpi) in (**c**); 9 (WT non-irradiated), 11 (WT 4 hpi), 6 (*actDrice* non-irradiated), and 11 (*actDrice* 4 hpi) in (**d**); 27 (WT) and 20 (*actDrice*) in (**g**); and 27 (WT 48 hpi), 20 (*actDrice* 48 hpi), 6 (*actDrice* 72 hpi), and 4 (*actDrice* 96 hpi) in (**h**). $^*p < 0.05$; $^{**}p < 0.01$; $^{***}p < 0.001$; $^{****}p < 0.0001$; ns, not significant. *p*-values in (**c**): $P < 0.0001$ (4 hpi vs. 24 hpi), $p < 0.0001$ (24 hpi vs. 48 hpi), and $p < 0.0001$ (4 hpi vs. 48 hpi); (**d**): $p = 0.0333$ (WT non-irrad. vs. WT 4 hpi) and $p = 0.0181$ (*actDrice* non-irrad. vs. *actDrice* 4 hpi); (**g**): $p < 0.0001$ (WT vs. *actDrice*); (**h**): $p = 0.0002$ (WT 48 hpi vs. *actDrice* 48 hpi), $p = 0.9559$ (*actDrice* 48 hpi vs. *actDrice* 72 hpi), $P = 0.0658$ (*actDrice* 72 hpi vs. *actDrice* 96 hpi), and $p = 0.0064$ (*actDrice* 48 hpi vs. *actDrice* 96 hpi).

leading to the complete elimination of the wing epithelium[89,90]. To determine whether DARE cell clones contribute to the formation of normal adult wings, we monitored the flies immediately after eclosion to identify at least some of the DARE cell clones before they are eliminated. Indeed, following larval-stage irradiation, some DARE cell-derived green clones could still be detected shortly after eclosion in the fly wings expressing the *$_D$DBS*/G-TRACE system, indicating that these clones contribute to functional wing development (Fig. 3e).

Compensatory proliferation by NARE cells fails to support normal tissue regeneration in the absence of DARE cells

The observation that DARE cell-derived clones occupy a large portion of the regenerated WID at 48 hpi suggests an important role of the DARE cells in tissue regeneration. However, the regenerated WID also contains radiation-induced non-Dronc-activating apoptosis-resistant epithelial (NARE) cells (indicated by 'dark' areas in Fig. 3biv). We therefore investigated whether the DARE cells are crucial for WID regeneration or if NARE cells can support normal regeneration in the absence of DARE cells. To achieve this, we first aimed to ablate the DARE cells by ectopically expressing a strong 'killer' gene in these cells. While cell ablation in *Drosophila* is commonly achieved by over-expressing pro-apoptotic proteins from the Reaper family, we opted to ectopically express a constitutively active effector caspase instead, to avoid potential unrelated effects, since Reaper proteins act upstream of Dronc activation. We therefore generated a constitutively active Drice transgene (*actDrice*) that strongly induces apoptosis upon ectopic expression (Supplementary Fig. 1c–e). Irradiated WIDs expressing the *$_D$DBS*/G-TRACE system along with a *UAS-actDrice* transgenic construct contained only a few predominantly red-labeled DARE cells and a few rare small clones both before irradiation and 4 hpi, indicating that already during development of the WID or shortly after irradiation, this combined system effectively triggers apoptosis in the DARE cells (Fig. 3fi, ii, d, and Supplementary Fig. 1g). Consistent with this, numerous, almost exclusively red-labeled DARE cells were detected at 24 hpi (Fig. 3fiii and Supplementary Fig. 1i). By 48 hpi, these cells were largely cleared from the tissue, which showed no DARE cell-derived clones (Fig. 3fiv, g). Importantly, the ablation of the DARE cells led to a significant reduction in WID area at 48 hpi (Fig. 3h). Notably, while DARE cell ablation resulted in a reduction of WID area at 4 hpi, no further reduction was observed at 24 hpi, supporting the idea that WID regeneration predominantly occurs between ~24–48 hpi (Supplementary Fig. 1h, j). We attribute the noisy quantifications at shorter time points after irradiation (e.g., 4 hpi) to the relatively small but variable numbers of DARE cells detected at that stage. In contrast, at later time points (24 and 48 hpi), when the numbers of DARE cells and clones significantly increase, the impact of developmental noise is reduced (Supplementary Fig. 1g, i).

One possible explanation for the reduced WID size at 48 hpi following DARE cell ablation is that regeneration is delayed due to a low starting cell number, and that NARE cells might compensate for the loss of DARE cells if given additional time. To test this idea, we first assessed pupariation timing in irradiated larvae from both WT and DARE cell-ablated backgrounds. Wandering 3rd instar larvae at 48 hpi were transferred to fresh vials, and pupation was scored at 72 and 96 hpi. While all WT larvae had pupated by 72 hpi, only 60% of DARE-ablated larvae had done so by this time, with an additional 20% pupating by 96 hpi (Supplementary Fig. 1f). However, despite this developmental delay, WID size in DARE-ablated larvae remained unchanged at 72 hpi and significantly declined by 96 hpi. These findings suggest that NARE cells are unable to compensate for the complete loss of DARE cells, even with extended regeneration time. Moreover, the further reduction in WID size at 96 hpi raises the possibility that complete DARE cell loss may compromise the survival or maintenance of NARE cells, contributing to the observed tissue regression (Fig. 3h). Together, these results highlight the indispensable role of DARE cells in driving compensatory proliferation during tissue regeneration, a function that NARE cells, on their own, are unable to fulfill.

Dronc activity is essential for DARE cell proliferation and WID regeneration

To explore the mechanisms underlying compensatory proliferation in DARE cells, we first investigated whether non-lethal Dronc activity is essential for their proliferation and tissue regeneration. To test this, we first aimed to specifically attenuate Dronc activity in the DARE cells after their appearance. We first tested several *dronc* RNAi and dominant-negative transgenes for their ability to suppress eye ablation induced by ectopic expression of the Reaper family protein Hid, and selected the strongest (RNAi) transgene to inactivate Dronc in DARE cells. This approach was also applied when choosing other apoptosis suppressors used in this study (Fig. 4a). It is important to note that gene inactivation in this system is never complete, as detection of DARE cells and/or expression of transgenes in these cells relies on prior Dronc activity to facilitate reporter cleavage. Nevertheless, down-regulation of *dronc* in DARE cells significantly reduced their proliferation at 24 hpi, similar to the effect observed upon DARE cell ablation, while having no significant impact at 4 hpi (Fig. 4b, c and Supplementary Fig. 1g, i). Likewise, no significant effect on total WID area was observed at 4 and 24 hpi, likely due to the overall reduction in WID size at both 4 and 24 hpi (Supplementary Fig. 1h, j). Importantly, *dronc* knockdown led to a significant reduction in the area occupied by DARE cells and their derived clones at 48 hpi, with markedly smaller clones occupying less of the WID region compared to WT counterparts (Fig. 4b-d). Furthermore, as observed in DARE cell-ablated WIDs at 48 hpi, the reduced proliferation of DARE cells following *dronc* knockdown was not compensated by increased NARE cell proliferation, resulting in a significant decrease in overall WID size (Fig. 4e). Taken together with the DARE cell ablation results, these findings highlight a

https://doi.org/10.1038/s41467-025-65996-2

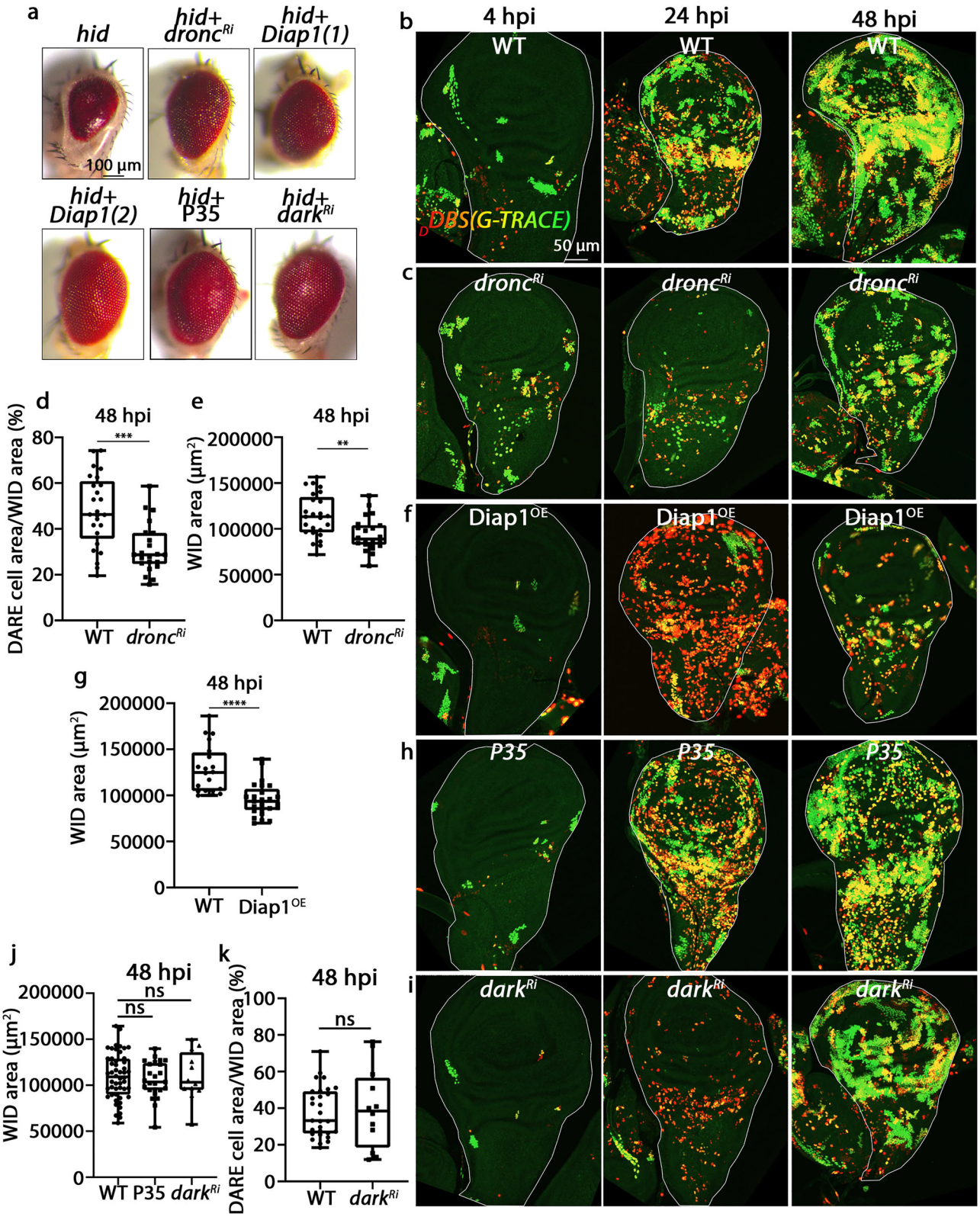

critical role for DARE cells in compensatory proliferation, wherein Dronc functions both cell-autonomously to regulate DARE cell proliferation and non-cell-autonomously to promote NARE cell proliferation. Given that Dronc activity is required for the initial cleavage of the $_{D}$*DBS* reporter and that the *dronc*^{Ri} is expressed in DARE cells only after this cleavage, the observed significant retardation in DARE cell proliferation likely even underestimates the true requirement of Dronc for DARE cell proliferation and tissue regeneration.

We next asked whether Dronc's role in compensatory proliferation depends on its catalytic activity, or if it instead functions through a non-catalytic mechanism, such as serving as a scaffold for other proteins. To address this question, we attenuated Dronc activity in the DARE cells by overexpressing the *Drosophila* caspase inhibitor Diap1, which binds to and inhibits the activities of both Dronc and the effector caspases[22,38–40,91]. Consistent with reduced Dronc activity, significant attenuation in DARE cell proliferation was observed,

Fig. 4 | Dronc, but not the effector caspases or the Dark apoptosome, is required for DARE cell proliferation and tissue regeneration. a Assessment of apoptosis-related RNAi lines and transgenes used in this study for suppressing Hid-induced apoptosis in *Drosophila* photoreceptor cells. The indicated transgenes were ectopically expressed in the retina using the *GMR-Gal4* driver. Two independently generated Diap1 transgenes were used: Diap1(1) (Fig. 4f) and Diap1(2) (Fig. 7i). Representative eyes of newly eclosed males are shown. **b**, **c**, **f**, **h**, **i** Irradiated WIDs expressing the transgenic combination described in Fig. 3a (control; **b**) or with DARE cell-specific knockdown of *dronc* (**c**) or *dark* (**i**), or overexpression of Diap1 (**f**) or P35 (**h**), were monitored at 4, 24, and 48 hpi. **d**, **k** Quantification of total DARE cell fluorescent area shown in (**b, c, i**) expressed as a percentage of total WID area. **e**, **g**, **j** The graphs depict total size in square micrometers of 48 hpi WIDs shown in (**b**, **c**, **f**, **h**, **i**). Statistical tests: Two-tailed unpaired Student's *t*-test (**b**, **e**, **g**, **k**); one-way ANOVA followed by Dunnett's multiple comparisons test (**j**). All data points, including outliers, are shown in box plot format. The lower and upper whiskers represent the minimum and maximum values, respectively; the center line denotes the median; and the lower and upper box bounds correspond to the medians of the lower and upper halves of the dataset. Each dot represents a single WID, reflecting the number of biologically independent WID samples (n). Numbers of WIDs examined were: 25 (WT) and 22 ($dronc^{Ri}$) in (**d**, **e**); 20 (WT) and 25 ($Diap1^{OE}$) in (**g**); 50 (WT), 25 (P35), and 12 ($dark^{Ri}$) in (**j**); and 29 (WT) and 12 ($dark^{Ri}$) in (**k**). $^{**}p < 0.01$; $^{***}p < 0.001$; $^{****}p < 0.0001$; ns, not significant. *p*-value in (**d**): $p = 0.0001$ (WT vs. $dronc^{Ri}$); (**e**): $p = 0.0022$ (WT vs. $dronc^{Ri}$); (**g**): $p < 0.0001$ (WT vs. $Diap1^{OE}$); (**j**): $p = 0.7721$ (WT vs. P35) and $p = 0.9994$ (WT vs. $dark^{Ri}$); (**k**): $p = 0.7519$ (WT vs. $dark^{Ri}$).

evidenced by the near absence of DARE cell-derived clones at 24 hpi, and the presence of only a few small clones at 48 hpi in irradiated WIDs expressing a *UAS-diap1* transgenic construct (*Diap1(1)* in Fig. 4a) along with the $_{D}$*DBS*/G-TRACE system (Fig. 4f). Interestingly, multiple, red-labeled DARE cells were detected at 24 hpi with only a few yellow cells and nearly complete absence of green cell clones following Diap1 expression (Fig. 4f). This is likely due to the potent inhibition of Dronc, which strongly attenuates DARE cell proliferation and clone formation, as well as Diap1's role as a potent apoptosis inhibitor, which prevents the natural death of some DARE cells by simultaneously inhibiting Dronc and the effector caspases. Finally, similar to the effect of *dronc* downregulation, DARE cells expressing Diap1 did not significantly affect total WID size at 4 or 24 hpi (Supplementary Fig. 1h, j), but they failed to support effective regeneration of the irradiated WID, as indicated by a significant reduction in WID size at 48 hpi (Fig. 4g). These results suggest that Dronc's catalytic activity, rather than a non-catalytic function, is required for compensatory proliferation.

Effector caspases and the apoptosome adapter protein Dark are dispensable in DARE cells for their proliferation and WID regeneration

During apoptosis, active Dronc cleaves and activates the effector caspases Drice and Dcp-1. Since Diap1 also inhibits these effector caspases, we next asked whether Dronc's role in promoting DARE cell proliferation and tissue regeneration depends on its own activity or on downstream effector caspase activity. To investigate this, we overexpressed the baculovirus protein P35 in DARE cells using the $_{D}$*DBS*/G-TRACE system. P35 potently inhibits apoptosis by binding to and inhibiting both Drice and Dcp-1, but not Dronc (Fig. 4a)[29,36,39,92–94]. However, P35 overexpression in DARE cells had no effect on cell proliferation and overall WID regeneration, as evidenced by normal clone formation and WID size at all time points (Fig. 4h, j and Supplementary Fig. 1h, j). Notably, although P35 overexpression did not affect clone formation, it did inhibit the natural death of some DARE cells due to its potent apoptosis-inhibiting properties, as evident by the accumulation of multiple individual, red- and yellow-labeled non-dividing DARE cells at 24 and 48 hpi (Fig. 4h). Interestingly, the P35-dependent surviving DARE cells do not induce visible AiP-associated tissue overgrowth, as might have been expected. This is likely due to both the timing and the low number of cells in this condition, which are insufficient to trigger an AiP effect. Previous studies have shown that AiP effects in WIDs can be clearly detected at approximately 72-96 hpi, whereas in our setup, P35 is expressed in DARE cells at 24 hpi, and we monitor the WIDs only 24 h later[73]. Collectively, we can conclude that effector caspases in DARE cells do not influence their proliferation or tissue regeneration. Thus, Dronc, but not effector caspase, drives DARE cell proliferation and tissue regeneration, indicating that Diap1's influence on this process is entirely attributable to its suppression of Dronc.

As a key activator of Dronc during apoptosis, the apoptosome Apaf-1 adapter ortholog Dark is essential for nearly all apoptotic events in *Drosophila*[31,32,34,35,37,95]. To determine if non-lethal activation of Dronc in DARE cells also requires Dark, we expressed a *dark* RNAi transgene (Fig. 4a) in the DARE cells using the $_{D}$*DBS*/G-TRACE system and monitored its effects on cell proliferation and WID regeneration. Unexpectedly, *dark* knockdown had no significant effect on DARE cell proliferation or WID regeneration at any of the examined time points after irradiation (Fig. 4i-k and Supplementary Fig. 1g–j). Therefore, non-lethal Dronc activation in DARE cells likely occurs independently of the Dark apoptosome.

The Dronc-interacting unconventional myosin Myo1D inhibits effector caspase activation in DARE cells

An important question arising from our findings is how DARE cells survive despite activating Dronc. To begin addressing this, we first investigated whether DARE cells exhibit effector caspase activity. To reduce background interference from the many dying cells and improve cellular resolution, we chose to express a genetic reporter specific to effector caspase activity exclusively in DARE cells, instead of using a global immunostaining approach for activated effector caspases. Called *CPV*, this well-established reporter of effector caspase activity consists of three components: an N-terminal mouse CD8 transmembrane domain, a short polypeptide of the human PARP protein containing a specific effector caspase cleavage site, and a C-terminal Venus fluorescent protein[29]. Upon apoptosis induction and cleavage by effector caspases, Venus is detached from the cell membrane and can be readily identified through the newly exposed PARP epitope (cPARP) using an anti-cleaved PARP antibody, as demonstrated by the expression of *CPV* in the pouch region of 3 hpi WIDs (Fig. 5a, b). Monitoring irradiated WIDs expressing the $_{D}$*DBS* reporter, along with *QUAS-Gal4* and *UAS-CPV* transgenic constructs, and immunostained for cPARP, revealed that most Venus-positive DARE cells exhibit low to no effector caspase activity at 4, 24, and 48 hpi (Fig. 5c, e). These findings may explain how DARE cells evade apoptotic death; however, it remains unclear why effector caspases are inactive in DARE cells despite the activation of Dronc.

Beyond its interaction with Dark during apoptosis, Dronc has been reported to bind other regulatory proteins involved in non-apoptotic functions. In both AiP models in the eye-antenna imaginal disc and in mature enterocytes of the adult posterior midgut, Dronc has been suggested to localize to the basal side of the cell membrane through interaction with the class I unconventional myosin, Myo1D[68,69]. While this localization is thought to facilitate Dronc's role in mediating extracellular signaling, we hypothesized that Myo1D binding could also inhibit Dronc's ability to effectively engage with and activate effector caspases. To test this idea, we knocked down *myo1D* in DARE cells using an RNAi from the TRiP library and monitored effector caspase activity using the *CPV* reporter (Fig. 5a). Strikingly, downregulation of *myo1D* increased effector caspase activity at both 24 and 48 hpi (Fig. 5d). This effect was particularly pronounced at 24 hpi, when the number of cPARP-positive cells significantly increased (Fig. 5d, e). Of note, the cPARP-positive cells appeared highly condensed compared to the Venus-positive, cPARP-negative cells, indicating that DARE cells, which activate effector caspases, undergo apoptosis.

https://doi.org/10.1038/s41467-025-65996-2

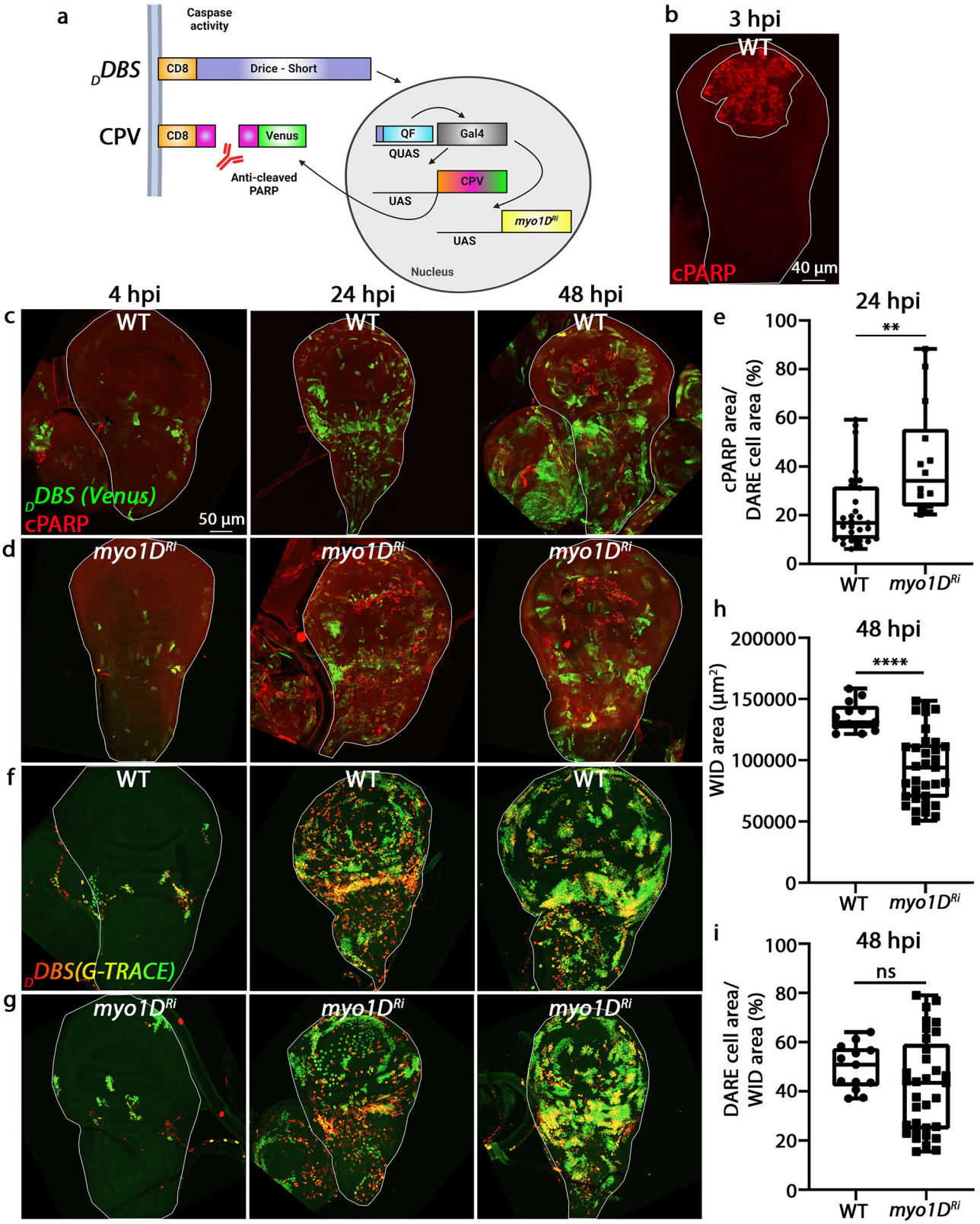

To strengthen this finding and assess the impact of *myo1D* downregulation on WID regeneration, we employed a second, independently generated RNAi transgene targeting *myo1D* from the VDRC KK library in the background of the *DBS*/G-TRACE system. Importantly, similar to *dronc* knockdown, downregulation of *myo1D* in the DARE cells led to a significant reduction in overall WID size at 48 hpi (Fig. 5f–h). Notably, although the area occupied by DARE cells and clones was not significantly reduced on average in *myo1D* knockdown WIDs, as opposed to the consistent reduction observed with *dronc* knockdown, these WIDs exhibited high variability. In multiple cases, the DARE cell area was reduced by more than half compared to control counterparts (Fig. 5f, g, i). Interestingly, these findings suggest that the Dronc-Myo1D interaction not only prevents inappropriate activation of effector caspases but may also be critical for mediating certain non-

Fig. 5 | *myo1D* knockdown in DARE cells triggers effector caspase activation and apoptosis. a Schematic of the *$_D$DBS* reporter combined with the *CPV* reporter of effector caspase activity and a *UAS-myo1D^{Ri}* transgene. Created in BioRender. Braun, T. & Yacobi-Sharon, K. (2025) https://BioRender.com/s6ebqxl. **b** An irradiated WID expressing the *CPV* reporter in the pouch region (using the *sal-Gal4* driver) and immunostained to reveal cleaved PARP (cPARP; red). **c**, **d** Irradiated WIDs expressing the transgenic combination described in (**a**) (control; **c**) or with DARE cell-specific *myo1D* knockdown (**d**), were immunostained for cPARP (red) and monitored at 4, 24, and 48 hpi. DARE cells are visualized by the Venus fluorescence of the *CPV* (green). **e** Quantification of the fraction of DARE cells expressing cPARP in WIDs represented in (**c**, **d**), measured as the cPARP-positive DARE cell area (red) relative to the total DARE cell area (green). **f, g** Irradiated WIDs expressing the transgenic combination described in Fig. 3a (control; **f**) or with DARE cell-specific *myo1D* knockdown (**g**), were monitored at 4, 24, and 48 hpi. **h** The graph depicts the total size of the 48 hpi WIDs shown in (**f**, **g**), presented as the total area in square micrometers (μm^2). **i** Quantification of the number of DARE cells and clones in 48 hpi WIDs, as represented in (**f**, **g**), is shown and presented as in Fig. 3g. Statistical tests: Two-tailed unpaired Student's *t*-test (**e**, **h**, **i**). All data points, including outliers, are shown in box plot format. The lower and upper whiskers represent the minimum and maximum values, respectively; the center line denotes the median; and the lower and upper box bounds correspond to the medians of the lower and upper halves of the dataset. Each dot represents a single WID, reflecting the number of biologically independent WIDs samples (n). Numbers of WIDs examined were: 29 (WT) and 14 (*myo1D^{Ri}*) in (**e**); and 13 (WT) and 33 (*myo1D^{Ri}*) in (**h**, **i**). $^{**}p < 0.01$; $^{****}p < 0.0001$; ns, not significant. *p*-value in (**e**): $p = 0.0012$ (WT vs. *myo1D^{Ri}*); (**h**): $p < 0.0001$ (WT vs. *myo1D^{Ri}*); (**i**): $p = 0.1914$ (WT vs. *myo1D^{Ri}*).

cell-autonomous effects of Dronc activity in DARE cells. It is important to note that *myo1D* is not a housekeeping gene, as null mutants are homozygously viable, with the only noticeable phenotype being the reversal of left-right asymmetry[96–98]. Taken together, these findings demonstrate that Myo1D plays a crucial role in protecting DARE cells from excessive caspase activation and apoptosis, thereby facilitating their proliferation and contributing to tissue regeneration.

The Dronc-interacting unconventional non-muscle myosin 7 A Crinkled promotes low levels of effector caspase activation in DARE cells

Another Dronc-binding protein, the unconventional non-muscle myosin 7 A (MYO7A) ortholog Myo7A/Crinkled, has been reported to promote Dronc activation in both apoptotic and non-apoptotic contexts[74]. Similarly, the eukaryotic translation initiation factor 3 subunit M (EIF3M) ortholog, Eif3m/Tango7, is reported to mediate some of Dronc's non-apoptotic activities at the cell cortex[99]. To explore the roles of Crinkled and Tango7 in regulating Dronc activity during compensatory proliferation, we expressed specific RNAi transgenes targeting these genes in DARE cells using the *$_D$DBS* reporter system and monitored effector caspase activity via DARE cell expression of the *CPV* reporter (as illustrated in Fig. 5a). Interestingly, while knockdown of *tango7* had no effect on the low residual activity of effector caspases in DARE cells at 24 hpi, downregulation of *crinkled* resulted in a significant reduction in the already low effector caspase activity in these cells (Supplementary Fig. 2a–d). Thus, whereas one unconventional myosin, Myo1D, inhibits effector caspase activation and ensures DARE cell survival, another, Myo7A/Crinkled, facilitates it, which may explain why not all DARE cells survive.

Of note, we also investigated whether differences in Drice and Dcp-1 protein expression between DARE and NARE cells could contribute to the survival of these populations. To this end, we immunostained 24 hpi WIDs from endogenously tagged fly lines (*drice::V5::TurboID* and *dcp-1::V5::TurboID*) using anti-V5 antibodies. Both proteins were expressed at similar levels and were uniformly distributed throughout the WIDs, with no detectable differences between DARE and NARE cells (Supplementary Fig. 2e, f). This observation is also consistent with previous findings from our lab, which reported similar levels of *drice* and *dcp-1* RNAs in non-irradiated 3rd instar larval WIDs[29].

Regulation of DARE cell proliferation and tissue regeneration by the MAPK family members JNK and p38

Studies of AiP and other Dronc-mediated paradigms, both apoptotic and non-apoptotic, have shown that the Jun N-terminal kinase (JNK) signaling pathway is activated downstream of Dronc[63,70,76,77,100–105]. To investigate possible involvement of the JNK pathway in proliferation of the DARE cells and tissue regeneration, we first knocked down *basket* (*bsk^{Ri}*), the sole *Drosophila jnk* gene, in flies expressing the *$_D$DBS*/G-TRACE system. Whereas no effect on irradiated WIDs was observed at 4 and 24 hpi following *jnk* downregulation (Supplementary Fig. 1g–j), a modest decrease in both the number and size of DARE cell-derived clones was revealed at 48 hpi (Fig. 6a–c, g). Intriguingly, while DARE cell ablation or inactivation of Dronc or Myo1D impaired tissue regeneration, inhibition of DARE cell proliferation upon *jnk* knockdown was compensated by an increase in NARE cell proliferation, as was reflected in the normal size of WIDs at 48 hpi (Fig. 6b, c, h).

The unexpectedly mild effect of JNK on compensatory proliferation led us to investigate the potential involvement of another MAPK (mitogen-activated protein kinase) family member, p38, which, like JNK, is known to play a key role in cellular stress responses[106–110] and has been implicated in various regeneration paradigms[111–114] (Fig. 6a). We specifically downregulated the two bona fide *Drosophila* p38 orthologs, *p38a* and *p38b*, in DARE cells. Notably, downregulation of *p38a*, but not *p38b*, led to a marked reduction in both the number and size of DARE cell-derived clones at 48 hpi, with no detectable effect at shorter time points (Fig. 6d, g, Supplementary Fig. 3a, b, d, e, and Supplementary Fig. 1g–j). Furthermore, similar to *dronc* knockdown, downregulation of *p38a* in DARE cells also resulted in a significant decrease in WID size at 48 hpi, suggesting that the non-cell-autonomous effect of DARE cells on NARE cells is mediated downstream of p38 signaling (Fig. 6b, d, h).

Since transgene expression in DARE cells is initiated only after the *$_D$DBS* reporter is cleaved by Dronc, by which time JNK and p38 signaling are already active, we employed an alternative genetic system to assess the maximal potential effects of *jnk* and *p38* downregulation on DARE cell induction and proliferation. In this system, the RNAi transgene is expressed independently of the *$_D$DBS* reporter throughout the entire posterior region of the WID, using the *hedgehog* (*hh*)-Gal4 driver. DARE cells were then visualized at 48 hpi using a *QUAS-mtdTomato* construct, which expresses membrane-targeted tdTomato following *$_D$DBS* reporter cleavage by Dronc and subsequent nuclear translocation of the QF transcription factor (Fig. 7a). Overexpression of either a dominant-negative form of JNK (JNK^{DN}) or the JNK inhibitor phosphatase Puckered (Puc)[115] in the posterior WID resulted in a marked reduction in both the number and size of DARE cell-derived clones, compared to the unmanipulated anterior region (Fig. 7b–d, b'–d'). Notably, the effect of Puc overexpression was more pronounced than that of JNK^{DN}, consistent with the notion that Puc is regulated by and may inhibit both JNK and p38 signaling pathways[116–119].

While these genetic data indicate an important role for p38 and JNK signaling in DARE cell proliferation, we next asked whether NARE cells might also rely on these pathways in a cell-autonomous manner. Since we are unable to specifically downregulate these pathways in NARE cells, we instead assessed JNK/p38 activity in both DARE and NARE cells at 24 hpi using the *TRE-RFP* reporter[120]. Notably, although *TRE-RFP* was originally designed to report JNK activity via the binding of Jun and Fos to the TRE synthetic sequence[120], several studies have shown that Jun and Fos can also be regulated by p38 signaling[121–123], suggesting that this reporter may reflect the combined activity of both JNK and p38 pathways. NARE cells were defined as those negative for both the *$_D$DBS* reporter (marking DARE cells) and cDcp-1 (marking

https://doi.org/10.1038/s41467-025-65996-2

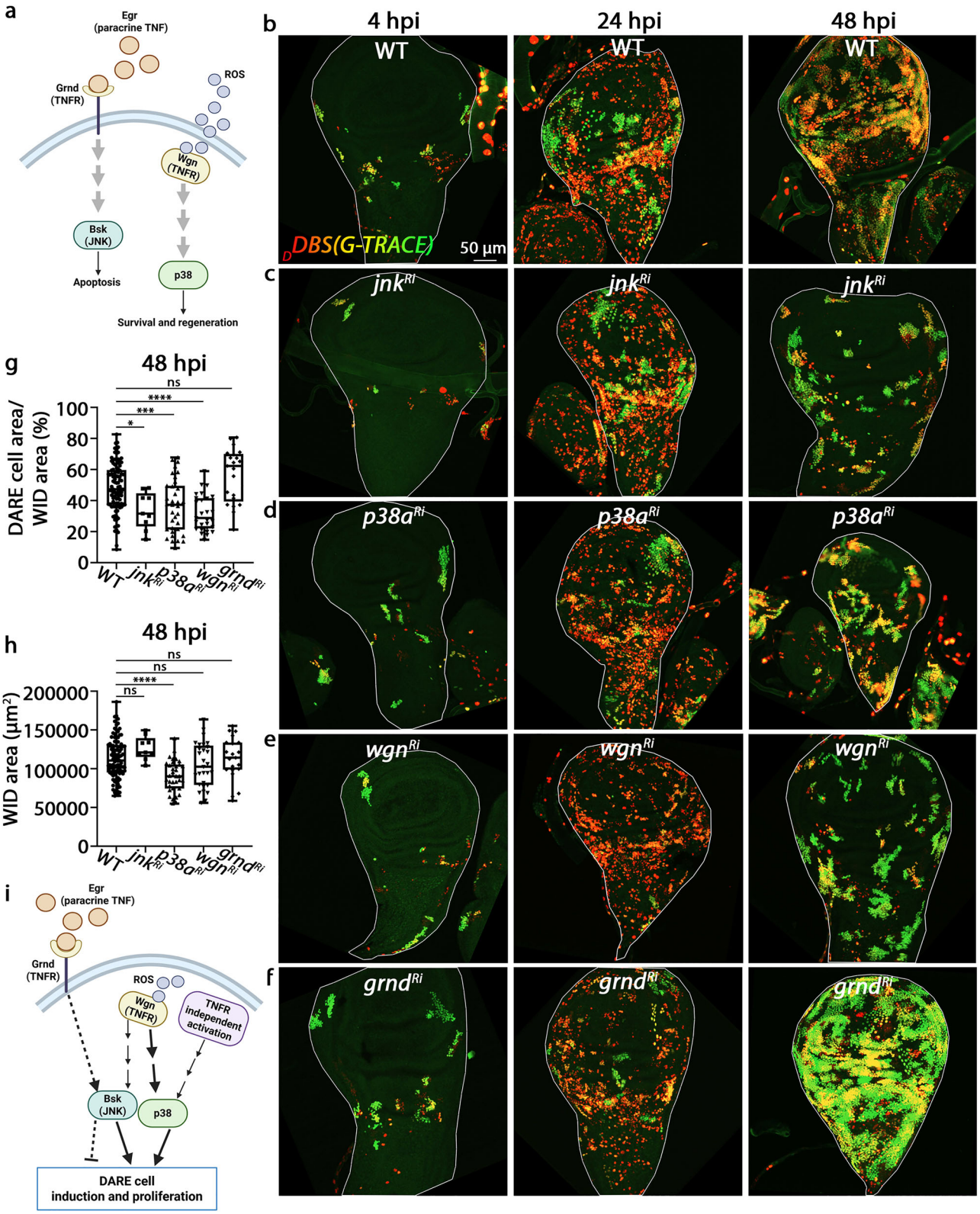

apoptotic cells). TRE-RFP signal was significantly higher in DARE cells compared to NARE cells, suggesting that, unlike DARE cells, NARE cells may not rely on p38/JNK pathway activations for their proliferation (Fig. 7k, l). Collectively, these findings support the conclusion that JNK and p38 signaling play an important role in promoting DARE cell proliferation and tissue regeneration.

The *Drosophila* p53 ortholog (Dp53) has previously been implicated in promoting Dronc-dependent cell proliferation within the context of AiP[76,124]. Dp53 and JNK have also been reported to form a positive feedback loop downstream of Dronc, which serves to amplify the initial apoptotic signal[125]. Given the involvement of Dronc, p38, and JNK in compensatory proliferation, we investigated whether Dp53 also contributes to DARE cell proliferation and tissue regeneration. However, knockdown of *dp53* specifically in DARE cells had no significant effect on the number of DARE cells or clones, nor on overall WID size at 48 hpi (Supplementary Fig. 3d, e). Notably, *dp53* knockdown resulted

Fig. 6 | JNK and p38 signaling pathways, together with antagonistic roles of the TNFRs, regulate the proliferation of DARE cells during compensatory proliferation. a A schematic summary of the TNFR > JNK/p38 signaling pathways based on a recent publication[114]. Created in BioRender. Braun, T. & Yacobi-Sharon, K. (2025) https://BioRender.com/66l1elw. **b**–**f** Irradiated WIDs expressing the transgenic combination described in Fig. 3a were monitored at 4, 24, and 48 hpi. The conditions included: controls (**b**) and DARE cell-specific knockdowns of *jnk* (**c**), *p38a* (**d**) *wgn* (**e**), or *grnd* (**f**). **g** Quantification of the number of DARE cells and their derivative daughter cells in 48 hpi WIDs, as represented in (**b**–**f**), is shown and presented as in Fig. 3g. **h** The graph depicts the total size of the 48 hpi WIDs shown in (**b**–**f**), presented as the total WID area (μm²). **i** Schematic summary of the results shown in this figure and in Supplementary Fig. 3. Created in BioRender. Braun, T. & Yacobi-Sharon, K. (2025) https://BioRender.com/66l1elw. Statistical tests: One-way ANOVA followed by Dunnett's multiple comparisons test (**g**, **h**). All data points, including outliers, are shown in box plot format. The lower and upper whiskers represent the minimum and maximum values, respectively; the center line denotes the median; and the lower and upper box bounds correspond to the medians of the lower and upper halves of the dataset. Each dot represents a single WID, reflecting the number of biologically independent WID samples (n). Numbers of WIDs examined were: 101 (WT), 9 (jnk^{Ri}), 35 ($p38a$Ri), 29 (wgn^{Ri}), and 21 ($grnd^{Ri}$) in (**g**, **h**). $^{*}p < 0.05$; $^{***}p < 0.001$; $^{****}p < 0.0001$; ns, not significant. *p*-values in (**g**): $p = 0.0252$ (WT vs. jnk^{Ri}), $p = 0.0004$ (WT vs. $p38a^{Ri}$), $p < 0.0001$ (WT vs. wgn^{Ri}), and $p = 0.1108$ (WT vs. $grnd^{Ri}$); (**h**): $p = 0.446$ (WT vs. jnk^{Ri}), $p < 0.0001$ (WT vs. $p38a^{Ri}$), $p = 0.384$ (WT vs. wgn^{Ri}), and $p > 0.9999$ (WT vs. $grnd^{Ri}$).

in a significant reduction in WID size at 4 hpi, but not at 24 hpi, and had no effect on the number of DARE cells or clones (Supplementary Fig. 1g–j). Since this reduction was even more pronounced than that observed following DARE cell ablation at 4 hpi WIDs, it may be attributed either to unrelated developmental delay specific to this fly line or to off-target effects in other cell types, within or outside the WID.

Opposing roles of TNF receptors in regulating DARE cell proliferation

In *Drosophila*, JNK activation is primarily triggered through the activation of two TNF receptors: Wengen (Wgn) and Grindelwald (Grnd)[126–131]. Interestingly, recent findings suggest that Grnd promotes TNF-induced apoptosis, while Wgn is required for apoptosis-induced cell survival and WID regeneration (Fig. 6a)[114]. Additionally, Grnd has been reported to facilitate overgrowth of undead epithelial tissue during AiP, likely through JNK activation[103]. We therefore decided to examine the potential involvement of TNF receptors in compensatory proliferation by knocking down *grnd* and *wgn* in the DARE cells. While knockdown of either receptor in irradiated WIDs expressing the $_{D}$*DBS*/G-TRACE system had no significant effects at 4 (*wgn*) or 24 (*grnd* and *wgn*) hpi, *grnd* downregulation showed a mild but significant trend toward enhanced DARE cell induction and proliferation at 4 hpi (Fig. 6e, f and Supplementary Fig. 1g–j). However, at 48 hpi, *wgn* knockdown in WIDs resulted in a significant reduction in both the number and size of DARE cell-derived clones, whereas *grnd* knockdown showed a mild, though non-significant, trend toward an increase in clone number and size (Fig. 6e-g). Given the *grnd* knockdown effect at 4 hpi, these results suggest that Grnd and Wgn may have opposing roles in regulating DARE cell proliferation, with Grnd acting negatively and Wgn positively. Measuring WID area size at 48 hpi revealed no change with *grnd* and *wgn* knockdowns (Fig. 6h). Collectively, these findings suggest that Wgn is the primary TNF receptor in DARE cells that promotes their proliferation, presumably through activation of p38 and JNK signaling pathways. However, the pronounced effect of p38 on both DARE and NARE cell proliferation and overall tissue regeneration suggests that p38 may also be activated through additional mechanisms, as previously proposed[132–137]. By contrast, Grnd seems to exert a mild inhibitory effect on DARE cells, although the downstream signaling mechanisms remain undefined (illustrated in Fig. 6i).

Drosophila possesses a single member of the TNF superfamily, Eiger (Egr)[138]. Given the involvement of TNF receptors in DARE cell proliferation, we investigated whether autocrine or paracrine TNF/Egr signaling from DARE cells contributes to compensatory proliferation. However, knockdown of *egr* specifically in DARE cells had no effect on the proliferation of either DARE or NARE cells, nor on overall tissue regeneration at all time points (Supplementary Fig. 3c–e and Supplementary Fig. 1g–j). In contrast, *egr* knockdown throughout the posterior region of the WID led to a moderate but significant increase in the number of DARE cells and clones compared to the unmanipulated anterior region (Fig. 7e, e'). These results suggest that, while DARE cells are not the source of TNF/Egr in this context, TNF/Egr may be secreted by either dying cells or NARE cells, acting in a paracrine manner to moderately inhibit DARE cell proliferation. This result aligns with the observed trend of negative regulation of DARE cell proliferation by Grnd, suggesting that paracrine TNF/Egr signals through Grnd on DARE cells to restrain their proliferation (Fig. 6i).

ROS produced by Duox and Nox in DARE cells promote their proliferation independently of hemocyte-derived mediators

Although both Grnd and Wgn can bind Egr, Wgn has been reported to do so with significantly lower affinity compared to the Grnd-Egr interaction[126]. Our findings that Wgn and Grnd-Egr act antagonistically to regulate DARE cell proliferation suggest that Wgn may be activated through a mechanism independent of TNF/Egr signaling. Consistent with this idea, a recent report suggests that Wgn can be activated independent of TNF/Egr by reactive oxygen species (ROS) during damage-induced tissue regeneration[114]. Furthermore, a key feature of AiP is the Dronc-dependent production of extracellular ROS by 'undead' cells, which attracts hemocytes to the tissue, where they secrete TNF/Egr to promote cell proliferation[69,70,103,139]. We therefore set out to investigate possible roles of ROS and hemocytes in promoting DARE cell proliferation. First, we downregulated the two major ROS-generating enzymes in *Drosophila*, Dual oxidase (Duox) and NADPH oxidase (Nox), specifically in DARE cells. While knockdown of both *nox* and *duox* resulted in a significant reduction in DARE cell numbers and clone size at 48 hpi, the effect of *duox* knockdown was more pronounced (Supplementary Fig. 3f–h). Consistent with the behavior of Wgn and JNK, no significant change in WID size was observed at 48 hpi (Supplementary Fig. 3f, g, i), and no effects were detected at the shorter time points of 4 and 24 hpi (Supplementary Fig. 1g–j).

To assess the potential involvement of hemocytes as mediators in compensatory proliferation, we ablated larval hemocytes by overexpressing the *actDrice* construct specifically in hemocytes using $Hml^{\Delta 2A}$-*Gal4*, a strong hemocyte-specific driver[140]. Following irradiation in an otherwise WT background, the already low number of hemocytes in the WID gradually declines from 4 hpi to 24 hpi and further to 48 hpi (Supplementary Fig. 3j). Upon *actDrice* expression, hemocyte numbers are dramatically reduced at all time points, with almost no hemocytes detectable in the WIDs (Supplementary Fig. 3j). Nevertheless, WID size remained unaffected, indicating that hemocytes are dispensable for compensatory proliferation in this context (Supplementary Fig. 3k). Together, these findings indicate that while ROS produced in DARE cells is essential for their proliferation and proper tissue regeneration, hemocytes are not required for compensatory proliferation.

Dying cells induce DARE cell formation downstream of effector caspase activation

Our finding that downregulation of *egr* in the posterior region of the WID, but not specifically in DARE cells, affects DARE cell induction raised the hypothesis that the source of TNF/Egr is either dying cells or NARE cells. To test whether dying cells influence DARE cell

https://doi.org/10.1038/s41467-025-65996-2

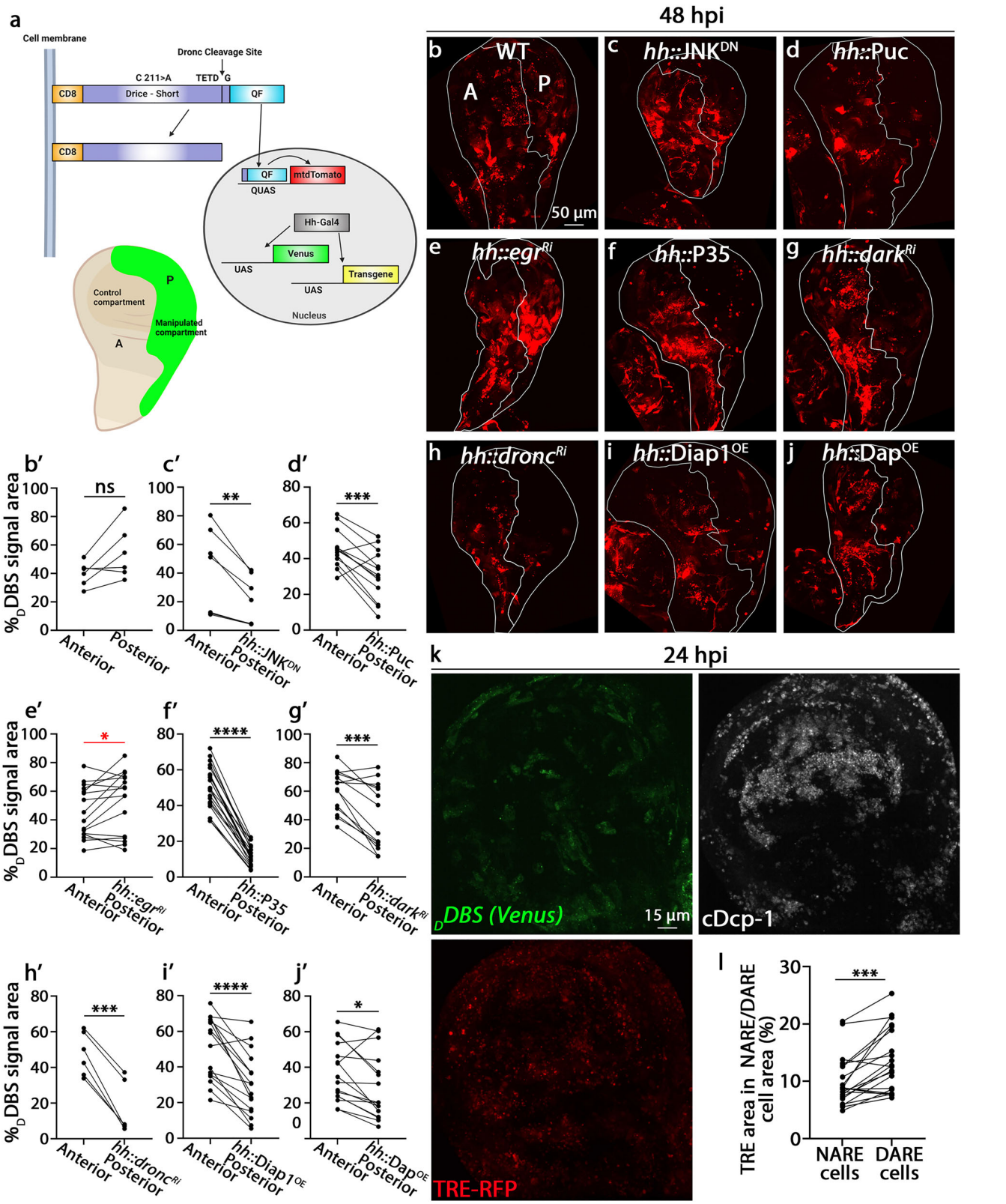

proliferation, we blocked apoptosis in the posterior WID region by either overexpressing P35 or knocking down *dark*. Notably, despite having no effect when applied specifically to DARE cells (Fig. 4h–k), both genetic manipulations led to a drastic reduction in DARE cell formation at 48 hpi (Fig. 7f, f′, g, g′). Similar results were also observed following *dronc* downregulation and Diap1 overexpression in the posterior WID (Fig. 7h, h′, i, i′). However, interpretation of these findings is more complex, as Dronc, and, by extension, its inhibitor Diap1, not only plays a key role in apoptosis but also cleaves the reporter and promotes the proliferation of both DARE and NARE cells. Finally, it is worth noting that while total WID size serves as a useful readout for assessing regeneration following DARE cell-specific manipulations, similar genetic manipulations applied to the entire posterior WID cannot be evaluated this way due to confounding

Fig. 7 | Dying cells induce the formation of DARE cells during compensatory proliferation. a Schematic of the dual binary system combining the *$_D$DBS* reporter with a *QUAS-mtdTomato* transgene to label DARE cells (red), together with an *hh-Gal4* for transgene expression in the WID posterior compartment. Created in BioRender. Braun, T. & Yacobi-Sharon, K. (2025) https://BioRender.com/nur2gq6. **b**–**j** Irradiated WIDs at 48 hpi of the genotype shown in (**a**) carrying either only a *UAS-GFP* transgene (**b**) or additionally the indicated transgenes (**c**–**j**). **b'**–**j'** Quantification of area occupied by DARE cells in the anterior and posterior compartments of the WIDs shown in (**b**–**j**). Results are presented as paired scatter plots, showing the percentage of area occupied by DARE cell clones in the anterior versus posterior compartments of each WID. Black and red asterisks represent a significant decrease or increase, respectively. **k** Evaluation of JNK/p38 pathway activity in DARE versus NARE cells with the JNK reporter *TRE-RFP* (red). DARE cells are labeled by the *$_D$DBS* reporter (Venus, green); dying cells are marked with cDcp-1 (white); the NARE cell area was calculated as the dark regions minus the area occupied by dying cells. **l** Quantification of JNK/p38 activity in DARE versus NARE cells in the WIDs shown in (**k**). Results are presented as a paired scatter plot, showing the percentage of TRE-RFP-positive area within DARE cell clones compared to the NARE cell area of each WID. Statistical tests: Two-tailed paired Student's *t*-test (**b'**–**j'**, **l**). All data points, including outliers, are shown as individual values. Numbers of WIDs examined were: 6 (WT, **b'**), 7 (*hh*::JNK^{DN}, **c'**), 13 (*hh*::Puc, **d'**), 16 (*hh::egr^{Ri}*, **e'**), 21 (*hh*::P35, **f'**), 14 (*hh::dark^{Ri}*, **g'**), 6 (*hh::dronc^{Ri}*, **h'**), 17 (*hh*::Diap1^{OE}, **i'**), 16 (*hh*::Dap^{OE}, **j'**), and 21 (**l**). *$p < 0.05$; **$p < 0.01$; ***$p < 0.001$; ****$p < 0.0001$; ns, not significant. *p*-value in (**b'**): p = 0.06 (WT); (**c'**): $p = 0.0067$ (JNK^{DN}); (**d'**): $p = 0.0009$ (Puc); (**e'**): $p = 0.0348$ (*egr^{Ri}*); (**f'**): $p < 0.0001$ (P35); (**g'**): $p = 0.0005$ (*dark^{Ri}*); (**h'**): $p = 0.0002$ (*dronc^{Ri}*); (**l'**): $p < 0.0001$ (Diap1^{OE}); (**j'**): $p = 0.0111$ (Dap^{OE}); (**l**): $p = 0.0002$ (NARE vs. DARE cells).

influences from the unmanipulated anterior region. We conclude that apoptotic cells in the surrounding tissue are required to promote DARE cell induction downstream of effector caspase activation.

Proliferative homeostasis between DARE and NARE cells ensures balanced compensatory growth of the tissue

At 48 hpi, DARE and NARE cells each occupy roughly half of the WID area. Our findings that dying cells promote DARE cell formation, while paracrine TNF/Egr negatively regulates these cells, suggest that the source of TNF/Egr is not the dying cells but rather the NARE cells, which may provide negative feedback to maintain a balanced proliferative equilibrium between the two populations. Given that NARE cells cannot properly compensate for the complete loss of DARE cells, or for the inactivation of Dronc or p38 in DARE cells, we next asked whether impaired, but not abolished, DARE cell proliferation would trigger overproliferation of NARE cells at the expense of DARE cells. To test this hypothesis, we sought to inhibit DARE cell proliferation downstream of Wgn>p38/JNK signaling by overexpressing Dacapo (Dap), the *Drosophila* Cyclin E/Cdk2 inhibitor[141,142], specifically in DARE cells. Whereas monitoring irradiated WIDs expressing the *$_D$DBS* reporter, the *QUAS-Gal4* adapter, a *UAS-Dap-GFP* transgene, and a *UAS-RedStinger* for DARE cell detection showed no significant effects at 4 hpi, a significant reduction in both the number and size of DARE cell clones became evident at both 24 and 48 hpi (Fig. 8a–c). Similar results were also observed upon Dap overexpression throughout the entire posterior region of 48 hpi WIDs (Fig. 7j, j'). Furthermore, we believe that the effect of Dap overexpression in DARE cells may be even more pronounced than observed, as the sparse and small clones detected at 24 and 48 hpi could result from either inefficient Dap expression in the originating DARE cells or mitotic recombination triggered by IR-induced double-strand DNA breaks, as suggested by the absence of GFP fluorescence in these clones (Fig. 8bii, iii). Importantly, despite the reduced proliferation of DARE cells, WIDs overexpressing Dap were able to maintain a normal overall size at 48 hpi, with a trend towards being slightly larger (Fig. 8d). This suggests that NARE cells overproliferated to compensate for the reduced proliferation of DARE cells. These findings also imply the existence of an additional regulatory mechanism that monitors WID size and terminates proliferation upon reaching normal dimensions, a process that may become disrupted when DARE cell fitness is impaired.

We next investigated whether disrupting the proliferative balance between the two cell populations affects WID differentiation and the final size of the adult wing. Monitoring young adult wings (~24 h after eclosion) from flies overexpressing Dap in DARE cells revealed only a modest increase in morphological abnormalities compared to irradiated control flies across all time points (Fig. 8e). Interestingly, however, wing size comparisons revealed a significant reduction in both female and male flies derived from Dap-overexpressing wandering 3rd instar larvae at 4 and 48 hpi, but not at 24 hpi (Fig. 8f, g). Therefore, although NARE cells can overproliferate to compensate for reduced DARE cell proliferation, disrupting the proliferative balance between the two populations mildly affects proper WID differentiation but significantly compromises final wing size.

NARE cell proliferation is enhanced at the interface with DARE cells

Given the proliferative balance between DARE and NARE cells, we next sought to directly assess the impact of DARE cells on NARE cell proliferation. To visualize mitotic cells within the regenerating tissue, irradiated WIDs expressing the *$_D$DBS*/G-TRACE system were immunostained with an antibody against Phosphohistone H3 (pHH3), a well-established marker of chromatin condensation during mitosis[143]. At 24 hpi, a time when multiple DARE cells are present, numerous mitotic cells were observed throughout the tissue (Fig. 9a). Closer examination, however, revealed that many of these dividing cells were located not within DARE cell clone masses but rather at their periphery (Fig. 9b). Furthermore, supporting the idea that DARE cells promote the proliferation of neighboring NARE cells, many pHH3-positive mitotic cells located at the periphery of DARE cell clones lacked fluorescent lineage markers, indicating they were NARE cells likely responding to mitogenic signals from adjacent DARE cells (Fig. 9b). Indeed, quantification at 24 hpi confirmed this trend: approximately 60-70% of mitotic cells at this stage were NARE cells, with the vast majority positioned within less than one epithelial cell diameter from DARE cells (Fig. 9c). Notably, at this stage, DARE cells occupy only ~30% of the WID area (Fig. 3biii, c), likely accounting to the observed higher number of dividing NARE cells. The granular appearance of red-labeled, newly emerging DARE cells is attributed to the G-TRACE RedStinger protein, rather than an intrinsic property of the cells themselves.

To visualize the spatial relationship between dividing NARE cells and neighboring DARE cells, we applied an expansion microscopy (ExM) protocol, which enlarged the tissue approximately fourfold and enabled high-resolution imaging of cell-cell proximity. This approach revealed that dividing NARE cells located at the DARE-NARE interface are in direct contact with adjacent DARE cells (Fig. 9d). Together, these findings strongly suggest that NARE cell proliferation is enhanced explicitly at the immediate interface with DARE cells.

Compromised proliferation, but not ablation, of DARE cells triggers NARE cell overproliferation

Our genetic findings collectively indicate that the interplay between DARE and NARE cells is essential for proper tissue regeneration, with Dronc playing a central role within DARE cells in maintaining proliferative homeostasis. To directly investigate the proliferative behavior of these two cell populations under conditions of disrupted balance, we first monitored the global proliferative index in the WID following irradiation. Using 5-ethynyl-2′-deoxyuridine (EdU) labeling to detect proliferating cells, based on S-phase DNA synthesis, in irradiated WT WIDs revealed a progressive increase in the number of

https://doi.org/10.1038/s41467-025-65996-2

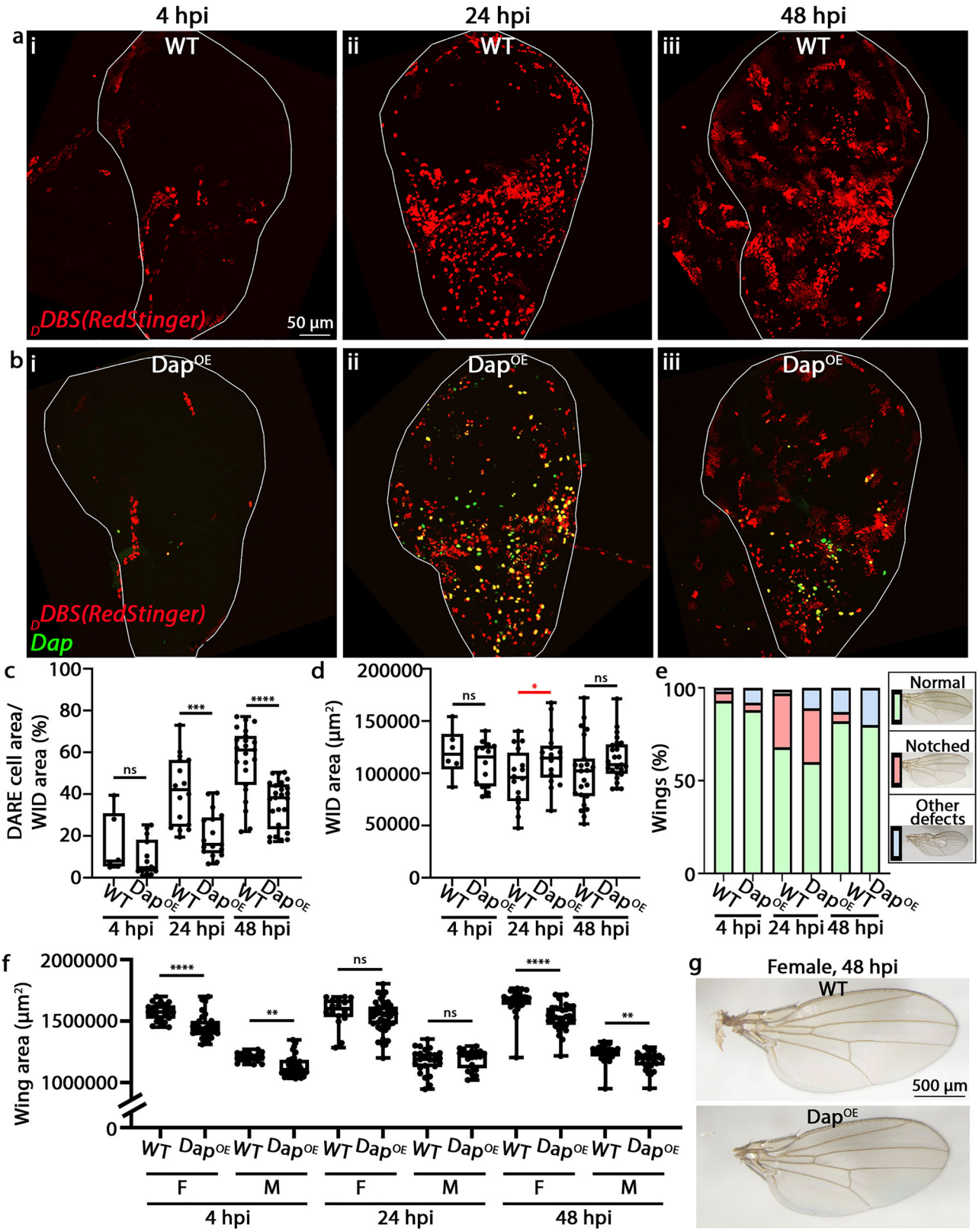

proliferating cells over time, peaking at 48 hpi (Fig. 9e). We next examined how the proliferative index of NARE cells is affected in WIDs where DARE cells are ablated (via *actDrice* expression) or where *dronc* or *myo1D* are knocked down, compared to the proliferative index observed under control conditions. Consistent with our genetic data indicating that DARE cells are essential for regenerative NARE cell proliferation, no significant change in the proliferative index was observed in DARE cell-ablated WIDs at 24 hpi (Fig. 9f). In contrast, *dronc* or *myo1D* downregulation in DARE cells, which we know is incomplete and still allows for the presence of some DARE cells and clones (Fig. 4c, d and Fig. 5g, i), led to increased NARE cell proliferation at 24 hpi (Fig. 9f). Therefore, overproliferation of NARE cells in response to reduced DARE cell proliferation requires the presence of at least some DARE cells and clones. Notably, disruption of the

Fig. 8 | Cell cycle-compromised DARE cells drive NARE cell overproliferation, restoring tissue size but impairing organ differentiation. a, **b** Irradiated WIDs containing the *$_D$DBS* reporter, *QUAS-Gal4* adapter, and *UAS-RedStinger*, with (**b**) or without (**a**) a *UAS-Dap-GFP* transgenic construct, were monitored at 4, 24, and 48 hpi. DARE cells are in red. **c** Quantification of total DARE cell fluorescent area shown in (**a**, **b**) expressed as a percentage of total WID area. **d** The graphs depict total size in square micrometers of WIDs shown in (**a**, **b**). **e**–**g** Overproliferation of WID NARE cells at the expense of DARE cells results in increased differentiation (**e**) and size (**f**, **g**) abnormalities in the adult wing. The graphs in (**f**) depict total size in square micrometers of adult wings shown in (**g**).Statistical tests: Two-tailed unpaired Student's *t*-test (**c**, **d**, **f**). All data points, including outliers, are shown in box plot format. The lower and upper whiskers represent the minimum and maximum values, respectively; the center line denotes the median; and the lower and upper box bounds correspond to the medians of the lower and upper halves of the dataset. Each dot represents a single WID, reflecting the number of biologically independent WIDs samples (n). Numbers of WIDs examined were: 6 (WT 4 hpi), 14 (Dap^{OE} 4 hpi), 16 (WT 24 hpi), 17 (Dap^{OE} 24 hpi), 23 (WT 48 hpi), and 25 (Dap^{OE} 48 hpi) in (**c**, **d**). Numbers of wings examined were: 24 (WT females 4 hpi), 29 (Dap^{OE} females 4 hpi), 18 (WT males 4 hpi), 34 (Dap^{OE} males 4 hpi), 16 (WT females 24 hpi), 46 (Dap^{OE} females 24 hpi), 25 (WT males 24 hpi), 20 (Dap^{OE} males 24 hpi), 30 (WT females 48 hpi), 31 (Dap^{OE} females 48 hpi), 23 (WT males 48 hpi), and 26 (Dap^{OE} males 48 hpi). *$p < 0.05$; **$p < 0.01$; ***$p < 0.001$; ****$p < 0.0001$; ns, not significant. *p*-values in (**c**): $P = 0.2373$ (WT 4 hpi vs. Dap^{OE} 4 hpi), $p = 0.0001$ (WT 24 hpi vs. Dap^{OE} 24 hpi), and $p < 0.0001$ (WT 48 hpi vs. Dap^{OE} 48 hpi); (**d**): $P = 0.3189$ (WT 4 hpi vs. Dap^{OE} 4 hpi), $p = 0.0425$ (WT 24 hpi vs. Dap^{OE} 24 hpi), and $p = 0.1067$ (WT 48 hpi vs. Dap^{OE} 48 hpi); (**f**): $p < 0.0001$ (WT females 4 hpi vs. Dap^{OE} females 4 hpi), $p = 0.0012$ (WT males 4 hpi vs. Dap^{OE} males 4 hpi), $p = 0.2935$ (WT females 24 hpi vs. Dap^{OE} females 24 hpi), $p = 0.5727$ (WT males 24 hpi vs. Dap^{OE} males 24 hpi), $p < 0.0001$ (WT females 48 hpi vs. Dap^{OE} females 48 hpi), and $p = 0.0078$ (WT males 48 hpi vs. Dap^{OE} males 48 hpi). Black and red asterisks represent significant decrease or increase, respectively.

proliferative balance by knocking down *wgn*, *duox/nox*, or *jnk* in DARE cells allows for restoration of normal WID size through compensatory NARE cell overproliferation. In contrast, knockdown of *dronc*, *myo1D*, or *p38*, although also leading to NARE cell overproliferation, fails to restore normal WID size. This suggests that the proliferative signal promoting NARE cell expansion originates from DARE cells and acts downstream of Dronc and p38 signaling.

DARE cell clones resist apoptosis induced by re-irradiation

The observation that DARE cells survive irradiation while many adjacent epithelial cells in the WID undergo apoptosis raises the question of whether this resistance is unique to early DARE cells or is also inherited by their cell progeny. To address this, we quantified cell death in double-irradiated WIDs. Larvae were first irradiated, allowed to regenerate for 48 h, re-irradiated, and analyzed 4 h later at the wandering 3rd instar stage. Quantification showed that, whereas a single irradiation resulted in dying epithelial cells occupying ~25% of the WID area at 4 hpi (duplicated from Fig. 1b), this percentage was reduced by about half (~13%) after the second irradiation, indicating that both DARE and NARE cells must exhibit increased resistance to subsequent irradiation (Fig. 10a). We next examined the relative contributions of DARE and NARE cells to the resistant cell population in double-irradiated WIDs carrying the *$_D$DBS*/G-TRACE system and immunostained for apoptosis using anti-cDcp-1 (Fig. 10b). Quantification was performed from images with only two fluorescent channels at a time. Figure 10b' shows the two G-TRACE channels: parental DARE cells (red), DARE progeny (green), and their overlap (yellow). However, when analyzing images displaying cDcp-1 (red) together with each individual G-TRACE channel (green), overlapping yellow apoptotic cells were extremely rare (Fig. 10b", b"'). On average, <30% of dying cells after double irradiation were DARE cells, with the majority being NARE cells (Fig. 10c). This corresponds to an approximate 7-fold and 3-fold decrease in sensitivity of DARE and NARE cells, respectively, to irradiation-induced apoptosis. Together, these results suggest the presence of a molecular 'memory' of apoptosis resistance in DARE cells, and to a lesser extent in NARE cells.

Discussion

In this study, we investigated the mechanisms underlying epithelial tissue regeneration by compensatory proliferation following IR. By employing a delayed genetic reporter for the activity of the initiator caspase Dronc, we identified a population of apoptosis-resistant epithelial cells, referred to as DARE cells, that are dispersed throughout *Drosophila* imaginal discs. In WIDs, these cells largely emerge at 24 hpi and undergo extensive proliferation during the subsequent 24 h. Regenerated imaginal discs at 48 hpi also contain another population of cells, termed NARE cells, which do not activate the reporter. Although this suggests that NARE cells, unlike DARE cells, do not activate Dronc, it is also possible that at least some of them lack part of the transgenic elements needed for DARE cell detection, due to mitotic recombination triggered by IR-induced double-strand DNA breaks. However, our findings, which demonstrate that DARE and NARE cells exhibit distinct proliferative characteristics, support the idea that NARE cells are largely a separate population of apoptosis-resistant epithelial cells that, along with the DARE cells, contribute to the regeneration of the imaginal disc.

Our findings provide the molecular and cellular foundation for a model of compensatory proliferation in epithelial tissues, as illustrated in Fig. 10d. According to this model, dying cells induced by IR emit signals that initiate or promote the formation of DARE cells. These DARE cells activate the initiator caspase Dronc in a manner independent of the Dark apoptosome. Myo1D binds to Dronc, potentially promoting its activation at the basal cell membrane while, importantly, preventing Dronc from being lethally activated by Dark and thereby averting effector caspase-mediated cell death. Dronc, along with JNK and p38 signaling, promotes DARE cell proliferation in a cell-autonomous manner to compensate for the cell loss. In parallel, downstream of Dronc and p38, DARE cells send a non-cell-autonomous signal that stimulates regenerative proliferation in NARE cells. These NARE cells, in turn, likely produce TNF/Egr, which acts in a negative feedback loop to moderately suppress DARE cell proliferation by binding to the TNF receptor, Grindelwald (Grnd), on DARE cells. p38/JNK signaling in DARE cells is likely activated through the alternate TNF receptor Wengen (Wgn), which in turn is activated by a TNF/Egr-independent mechanism, presumably via ROS produced within DARE cells. This bidirectional signaling establishes a proliferative balance between the two cell populations, ultimately regenerating the tissue with each population occupying approximately half of the WID (Fig. 10ei). If this balance is disrupted, such that DARE cell proliferation is compromised but not entirely lost, NARE cells compensate by overproliferating (Fig. 10eii). However, if DARE cells are completely ablated, NARE cells fail to increase their proliferative rate, indicating that their regenerative proliferation depends on the presence of DARE cells (Fig. 10eiii).

Whereas a positive amplification loop between JNK signaling and Dronc activation has been previously demonstrated[125,144,145], the mechanism by which Dronc activation occurs independently of the Dark apoptosome remains unclear. Furthermore, it is still uncertain whether such a mechanism is also linked to the ability of cells to activate Dronc while remaining alive (i.e., through binding to Myo1D). Dark-independent Dronc activation has been reported in other systems. For instance, Tango7 modulates Dronc levels and activity independent of Dark by sequestering it to the cell cortex during some non-apoptotic processes[99,146,147]. Additionally, Dronc has been shown to interact with Myo1D in 'undead' salivary gland and imaginal disc cells during AiP, as well as in enterocytes of the adult midgut[68,69]. This interaction sequesters Dronc to the basal side of the plasma

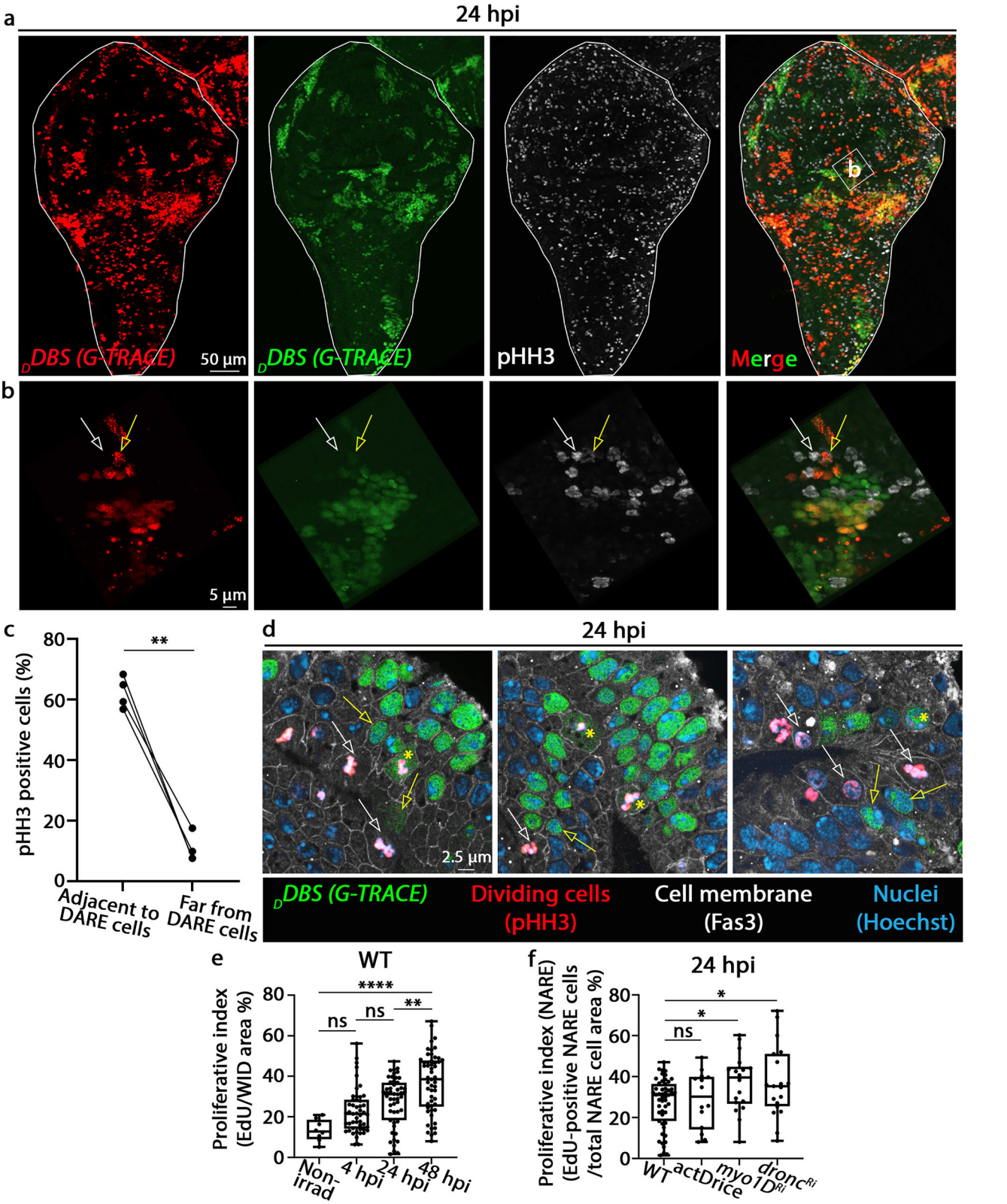

membrane, where it exhibits minimal co-localization with Dark, which mainly resides in the cytoplasm, hence suggesting that Dronc is largely separated from Dark in these cellular contexts[69]. Importantly, our findings suggest that the Dronc-Myo1D interaction is crucial for preventing unwanted excessive effector caspase activation and apoptosis in DARE cells. This provides evidence for a mechanism by which normal cells can activate Dronc while remaining alive. Additionally, it implies that the expression levels of Myo1D in WID epithelial cells may determine whether they undergo apoptosis or transform into DARE cells after irradiation. Interestingly, MYO1D has been implicated in tumor growth and an increased risk of malignancy by anchoring EGFR family members to the plasma membrane, suggesting that this motor protein plays a conserved role in the membrane sequestration of proteins associated with cell survival and growth[148,149].

Fig. 9 | NARE cell proliferation rate depends on the presence of DARE cells and their proliferation state. a Irradiated WIDs expressing the G-TRACE system in DARE cells (as described in Fig. 3a) were immunostained with anti-Phosphohistone H3 (pHH3; white) to mark proliferating cells. Shown is a representative WID at 24 hpi displaying DARE cells (red) and clones (green). **b** Enlargement of the boxed region in (**a**). A pair of adjacent DARE (yellow arrow) and NARE (white arrow) dividing cells is visualized. **c** Quantification of dividing NARE cells located either less (adjacent) or more (far) than one average cell diameter away from DARE cells in WIDs represented in (**a**). Results are presented as a paired scatter plot, indicating the percentage of dividing NARE cells in each location. Measurements were performed on the enlarged images (**b**). **d** Super-resolution images from 24 hpi WIDs, stained to visualize DARE cells (green), dividing cells (pHH3, red), cell borders (Fasciclin 3, white), and nuclei (blue), prepared using an expansion microscopy (ExM) procedure. DARE cells (yellow arrows) located adjacent to dividing NARE cells (white arrows) are visualized. Asterisks denote dividing DARE cells. **e** Quantification of the total WID area occupied by proliferating cells (EdU-positive) at all time points, expressed as the percentage of dividing cells within the total WID area. **f** The graphs depict the percentage of proliferating NARE cells (EdU-positive) in 24 hpi WIDs expressing the G-TRACE system to visualize DARE cells, expressed as the percentage of dividing NARE cells within the total NARE cell area. Statistical tests: Two-tailed paired Student's *t*-test (**c**); one-way ANOVA followed by Tukey's multiple comparisons test (**e**); one-way ANOVA followed by Dunnett's multiple comparisons test (**f**). Data points in (**e**, **f**), including outliers, are shown in box plot format. The lower and upper whiskers represent the minimum and maximum values, respectively; the center line denotes the median; and the lower and upper box bounds correspond to the medians of the lower and upper halves of the dataset. Each dot represents a single WID, reflecting the number of biologically independent WID samples (n). Numbers of WIDs examined were: 4 (**c**); 8 (non-irradiated), 49 (4 hpi), 51 (24 hpi), and 53 (48 hpi) in (**e**); and 51 (WT), 14 (*actDrice*), 18 (*myo1D*^{Ri}), and 19 (*dronc*^{Ri}) in (**f**). *$p < 0.05$; **$p < 0.01$; ****$p < 0.0001$; ns, not significant. *p*-value in (**c**): p = 0.0014 (Adjacent to vs. Far from DARE cells); (**e**): $p = 0.1985$ (non-irradiated vs. 4 hpi), $p = 0.2401$ (4 hpi vs. 24 hpi), $p = 0.0013$ (24 hpi vs. 48 hpi), and $p < 0.0001$ (non-irradiated vs. 48 hpi); (**f**): $p = 0.9723$ (WT vs. *actDrice*), $p = 0.0326$ (WT vs. *myo1D*^{Ri}), and $p = 0.0209$ (WT vs. *dronc*^{Ri}).

There are at least two significant conceptual cellular distinctions, along with key molecular differences, between AiP and compensatory proliferation. First, AiP in imaginal discs is typically studied under 'undead' cell conditions, where apoptosis is initiated but execution is blocked, and conclusions are extrapolated to dying cells. In contrast, compensatory proliferation is driven by naturally apoptosis-resistant cells, namely DARE cells. Second, in AiP, 'undead' cells, and by extension, dying cells, directly emit mitogenic signals to stimulate the proliferation of surrounding cells. In compensatory proliferation, however, dying cells act indirectly by inducing or activating DARE cells, which not only proliferate themselves but also serve as the source of proliferative signals that promote NARE cell expansion. At the molecular level, in the context of AiP, Dronc activity within dying cells mediates non-cell-autonomous proliferation in neighboring cells[38,64,65,68,69,71,76,77,103,150]. In contrast, during compensatory proliferation, Dronc regulates the proliferation of both DARE and NARE cells, acting cell-autonomously within DARE cells and non-cell-autonomously to promote proliferation of surrounding NARE cells. Furthermore, in AiP, Duox in 'undead' cells generates extracellular ROS that recruits hemocytes. These hemocytes release TNF/Egr, which binds to Grnd on the 'undead' cells, activating JNK signaling that enhances Dronc activity and drives non-cell-autonomous proliferation[63,68,70,73,101,103,150,151]. In contrast, during compensatory proliferation, both p38 and JNK signaling pathways, along with Duox, Nox, and Wgn, function within DARE cells to promote cell-autonomous proliferation. In this context, hemocytes are dispensable, and TNF/Egr, likely secreted by NARE cells, acts through Grnd on DARE cells to moderately inhibit their proliferation. Conversely, a pro-proliferative signal originating from DARE cells, acting downstream of Dronc and p38, promotes NARE cell proliferation. Note that the dual regulation and function of the JNK signaling in compensatory proliferation (Fig. 10d) is perhaps not surprising, given that this pathway has long been recognized for its remarkable versatility[152–155]. Likewise, in *Drosophila*, multiple studies have shown that JNK can function as either a pro-apoptotic or pro-proliferative signal, depending on the physiological context[144,145,156].

Since Egr is the sole TNF ligand in *Drosophila*, our data raise the possibility that Wgn activation in DARE cells occurs independently of TNF/Egr binding. Interestingly, this is consistent with a recent report showing that Wgn promotes cell survival and tissue regeneration following damage via activation by ROS, in contrast to Grnd, which is activated by TNF/Egr to induce apoptosis[114]. That study also positioned p38 downstream of Wgn. In line with this, we observed a significant role for both Wgn and p38 in promoting DARE cell proliferation and tissue regeneration. However, while the previous report implicates dying cells as the primary ROS producers[114], our data demonstrate that both Duox and Nox, the main ROS-generating enzymes, are required within DARE cells to support their proliferation. Therefore, although we cannot exclude the possibility that DARE cells may also respond to ROS generated by dying cells, our findings support previous reports suggesting that ROS can promote ligand-independent activation of TNF receptors, such as Wgn[114,157–159].

The role of Myo1D in AiP and compensatory proliferation is particularly intriguing. While Myo1D has been reported to sequester Dronc to the plasma membrane during AiP, potentially enhancing Dronc's non-cell autonomous proliferation effects[68–70], our study suggests an additional critical function. The Myo1D-Dronc interaction also prevents excessive effector caspase activation and cell death in DARE cells. Thus, Myo1D's role extends beyond facilitating the sequestration of Dronc at the cell cortex for its non-cell-autonomous functions during AiP, also serving to protect DARE cells from apoptosis. Interestingly, the detection of Dronc at the plasma membrane in 'undead' cells during AiP suggests that even in the context of cell death, a fraction of Dronc may be positioned in a way that facilitates the secretion of signals for the induction of DARE cells. Supporting this idea, we find that blocking apoptosis by ectopic expression of P35 or downregulation of Dark in the posterior region of the WID, but not in DARE cells, significantly inhibits induction of DARE cells, implying that dying cells actively secrete signals required for DARE cell activation. Notably, this signal appears to act downstream of effector caspase activation, rather than by Dronc, resembling a unique form of AiP previously described in the eye region of the eye-antenna imaginal disc[64]. Future studies aimed at identifying the signals that trigger DARE cell formation will be essential for clarifying the specific role of dying cells in initiating compensatory proliferation through DARE cell induction.

Regeneration and overgrowth of WIDs following irradiation or tissue injury have previously been attributed to epithelial cells that activate effector caspases but escape apoptosis; therefore, no definitive role has been assigned to caspases in this context[62,160–162]. Furthermore, it has been proposed that the surviving cells do not arise at random but are born at specific locations within the developing WID[62,160,162]. However, our findings indicate that the initiator caspase Dronc is essential for the proliferation of surviving cells. Moreover, the emerging DARE cells, particularly around 24 hpi, are dispersed throughout the WID, rather than originating from specific regions, with only minimal clustering of DARE cell clones observed just beneath the pouch area. A plausible explanation for these discrepancies may lie in the different caspase activity reporters used and variations in their expression setups. In contrast to the *$_{D}$DBS* reporter used in our study, those studies employed the CaspaseTracker or its closely related counterpart, CasExpress, both of which were designed to detect effector caspase activity[163,164]. However, these reporters might not be specific to effector caspase activity and could also be cleaved by

https://doi.org/10.1038/s41467-025-65996-2

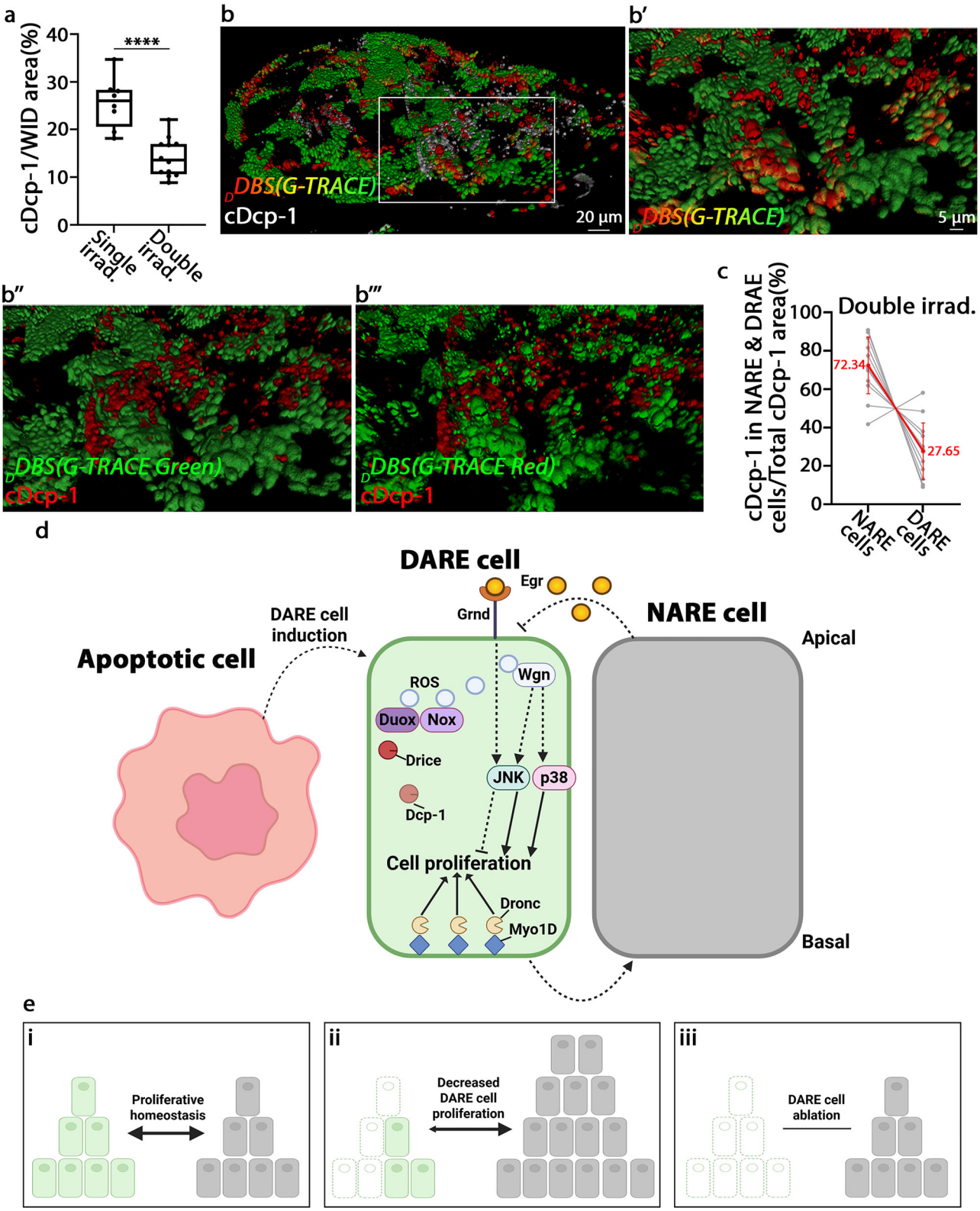

Dronc. Supporting this, it has been shown that overexpression of P35, which potently inhibits effector caspase activity but not Dronc activity, did not completely block CasExpress reporter activation in the eye imaginal disc[164]. Furthermore, those reporters contain a caspase-3-binding and cleavage domain from Diap1, with a DQVD cleavage site, linking an N-terminal transmembrane domain to a C-terminal Gal4[164]. Although Dronc cleaves itself at the TQTE site and cleaves effector caspases at the TETD site, screening of synthetic combinatorial tetrapeptide libraries with aspartate at the P1 position revealed that Dronc has a strong preference for valine at the P2 position. A broader range of amino acids is tolerated at the P3 and P4 positions, including glutamine and aspartate, respectively[36]. Therefore, it is plausible that the CasExpress and CaspaseTracker reporters detect both effector and initiator caspase activities, possibly with varying efficiencies for each caspase. This may explain why it was previously believed that surviving cells exhibit past effector caspase activity, rather than initiator caspase

Fig. 10 | DARE cell clones are resistant to re-irradiation-induced apoptosis. **a** Quantification of dying cells in irradiated WIDs, as shown in Fig. 1b, was performed 4 h after either the first (single) or second (double) irradiation, expressed as the percentage of dying cell area relative to the total WID area. **b** A representative irradiated WID expressing the *$_{D}$DBS*/G-TRACE system (as in Fig. 3a), re-irradiated and dissected as in (**a**), and immunostained with anti-cDcp-1 to mark dying cells (white). DARE cells and their derived clones are shown in red and green, respectively; overlap appears yellow. (**b′-b‴**) Enlargements of the boxed region in (**b**) with each panel displaying only two channels at a time to visualize overlap: DARE cells (red) and clones (green) labeled by G-TRACE (**b′**); DARE cell clones (green) and cDcp-1 (red) (**b″**); DARE cells (green) and cDcp-1 (red) (**b‴**). **c** A paired scatter plot quantifies cDcp-1-positive dying DARE and NARE cells 4 h after the second irradiation, expressed as their percentages within the total dying cell population in a WID. To ensure accuracy, 20 optical Z-slices were analyzed per WID to measure the overlaps. Statistical tests: Two-tailed unpaired Student's *t*-test (**a**). Graphs were generated and presented as in Fig. 1b. Numbers of WIDs examined was 8 (single irradiation) and 12 (double irradiation) in (**a**). ****$p < 0.0001$. In (**c**), all data points, including outliers, are shown as individual values; red indicates the mean (dots) with SD (whiskers). *p*-value in (**a**): $p < 0.0001$ (Single irradiation vs. Double irradiation). **d** A model of WID regeneration through compensatory proliferation following irradiation. The illustration depicts three adjacent cells: a dying cell, a DARE cell, and a NARE cell. Signaling pathways and components identified in this study are shown within the DARE cell, with arrows indicating activation and T-bars indicating inhibition. Dashed lines represent proposed interactions based on this study and the literature. A detailed explanation of the model is provided in the *Discussion*. **e** Illustrations showing the interplay between DARE and NARE cells during (i) normal proliferative homeostasis, (ii) reduced DARE cell proliferation, and (iii) complete absence of DARE cells. Illustrations in (**d**, **e**) were created in BioRender. Braun, T. & Yacobi-Sharon, K. (2025) https://BioRender.com/jtk6e8b.

activity, while also accounting for the less pronounced proliferation of surviving cells observed in those studies.

Another apparent discrepancy concerns the role of p53 in regeneration through compensatory proliferation. Two previous studies by the same group report contradictory findings: one proposing that compensatory proliferation depends on Dronc activity[76], and the other suggesting that it occurs independently of caspases[165]. Importantly, our study indicates that p53 has no essential cell-autonomous role in DARE cell compensatory proliferation, even though Dronc activity in these cells is crucial for their proliferation. The finding that Dronc activation in DARE cells is independent of Dark, and thus distinct from its activation during radiation-induced apoptosis, where it requires both Dark and p53, is consistent with our observation that p53 is not required for the proliferation of these cells. Therefore, a possible explanation for the apparent discrepancy is that p53 fulfills at least two roles in promoting compensatory proliferation after irradiation: first, by activating caspases and promoting apoptosis, as dying cells induce DARE cell formation; and second, as a provocative hypothesis, that p53 may function in NARE cells, which by definition do not activate Dronc. These distinct roles of p53 may therefore account for the apparent inconsistency in its reported net effects on compensatory proliferation in imaginal discs.

Understanding the mechanisms underlying compensatory proliferation following ionizing irradiation is crucial for both advancing our knowledge of tissue regeneration and addressing its connection to cancer[57]. Key characteristics of cancer cells are their ability to evade apoptosis and proliferate uncontrollably[166]. Indeed, several key factors associated with compensatory proliferation identified in the current study have previously been shown to promote tumor formation when dysregulated. Myo1D was previously shown to be essential for neoplastic tumor growth and invasion in *scrib$^{-/-}$Ras^{V12}* cells, a function originally attributed to its role in promoting Dronc localization to the plasma membrane[69]. However, our findings suggest that Myo1D may also contribute by preventing excessive effector caspase activation and apoptosis. Furthermore, expression of both MYO1D and MYO7A was linked to tumor growth and increased risk of malignancy[148,149,167]. The role of JNK in promoting tumor formation has also been demonstrated across various cancer models[110,168–171], including in *Drosophila*[63,100,104,144,172–175]. Given that most current anticancer therapies, including IR, induce apoptotic cell death[176–180], and that approximately two-thirds of cancer patients receive radiotherapy[181–184], understanding how certain cells resist radiation-induced apoptosis and subsequently proliferate is critical. Such insights could improve our understanding of cancer recurrence following treatment[185–188] and guide the development of more targeted and effective therapeutic strategies.

Methods

Fly strains

For a comprehensive list of the fly lines used in this study, please refer to the key resources table (Supplementary Table). The control lines used in the experiments share the same genetic background as the tested lines, except for the specific conditions being tested. These control lines are typically referred to as wild type (WT). The flies were reared at 25 °C.

Generation of the constitutively active Drice (*actDrice*) construct

A 935 bp fragment encoding the large and small subunits of Drice, excluding the prodomain, was PCR amplified from a full-length *drice* cDNA clone using the following primers: a forward primer, 5′-AATGCGGCCGCATGGCCCTGGGCTCCGTGGGAT-3′, which includes an ATG transcription start site and a NotI restriction site, and a reverse primer, 5′-CCAAGGTACCGCCAGCGGCCC-TCAAACCC-3′, which includes a KpnI restriction site. This fragment was then directionally subcloned into the NotI and KpnI sites of the *pUASTattB* plasmid, resulting in the *pUAST-NoPro-drice* plasmid. A 66 bp DNA fragment of the viral P2A sequence was PCR amplified from a plasmid provided by Prof. Yosef Shaul (in our department), using the following primers: a forward primer, 5′-ACCATGCAGCGTTCTCAGACGGAAACCGATGG AAGCGGAGCTACTAACTT-3′, and a reverse primer, 5′-TGGAATCTTG-TAGCTCATCGAGGAGTCGCCAGGTCCAGGGTTCTCCTC-3′. Both primers included *drice* overhang sequences, which facilitated the insertion of the amplified P2A fragment into the *pUAST-NoPro-drice* plasmid, between the large and small subunits of Drice, using restriction-free cloning. The P2A fragment was inserted at position 609 of the *NoPro-drice* sequence, immediately following the TETD tetrapeptide at the end of the large subunit.

Transgenic flies were generated via φC31-mediated site-specific transgenesis, with injections performed by BestGene Inc. (Chino Hills, CA, USA). The transgene was inserted into the attP40 site on the second chromosome.

Immunostaining procedures and imaging

All *Drosophila* larvae were irradiated with a dose of 20 Gy X-rays using the XRAD 320 X-ray unit from Precision X-ray (USA), except for the experiment shown in Fig. 3e, where a dose of 10 Gy X-rays was used to facilitate recovery of adult flies.

Imaginal discs were dissected from third instar larvae either before irradiation or at various time points afterward. The order of imaginal disc dissections by genotype was randomized for each experiment. After dissection, the imaginal discs were fixed in 4% paraformaldehyde (PFA) in PBS for 20 min at room temperature, then washed three times in PBX (PBS with 0.1% Triton X-100) for 10 min each.

To minimize variability that might derive from mounting, all samples were prepared by the same individual using a standardized and consistent protocol. Briefly, about 20 WIDs were aligned on a slide in a drop of PBS. The PBS was gently removed using Whatman filter paper, after which 10 μL of mounting medium was added adjacent to

the aligned WIDs. A coverslip was then placed at a 45° angle and allowed to lower gradually by gravity, ensuring even distribution of the mounting medium. Importantly, multiple WIDs from each experimental group were mounted on the same slide to allow direct comparison, and each experiment included at least two biological replicates.

Imaging was performed using a Dragonfly 505 spinning disk confocal system (Andor Technology PLC). Images were captured with a Sona 6 sCMOS camera mounted on a Leica DMi8 inverted microscope.

Immunostaining of the imaginal discs was performed on the washed, fixed samples. The discs were first incubated in a blocking solution of 1% BSA in PBS for 1 h at room temperature, then incubated overnight with a primary antibody diluted in 1% BSA/PBS at 4 °C. The samples were then washed in PBX, incubated with the secondary antibody for 1 h at room temperature, washed again in PBX, and finally mounted. In experiments involving multiple time points, samples were stained and mounted together at the latest time point for comparison.

To visualize the adult wing in Fig. 3e, flies with unfurled wings were collected soon after eclosion and kept at room temperature until the wings fully expanded. The wings were then collected within a few minutes of unfurling, mounted, and imaged immediately.

Expansion microscopy (ExM)

Wing disc expansion protocol. The wing disc expansion protocol was adapted from ref. 189. Bottles containing larvae were irradiated with 20 Gy, and 3rd instar larvae were dissected for WID tissue at 24 hpi. Wing discs were fixed and stained following a standard wing disc immunostaining protocol. Following immunostaining, samples were incubated in 1 mM MA-NHS (methacrylic acid N-hydroxysuccinimidyl ester; Sigma-Aldrich, 730300) in PBS for 1 h at RT, followed by 3 × 20 min PBS washes. Samples were then incubated in monomer solution [2 M NaCl, 8.625% sodium acrylate (Sigma-Aldrich, 408220), 2.5% acrylamide (Bio-Rad, 1610140), 0.15% bisacrylamide (Bio-Rad, 1610142) in PBS] for 1 h at 4 °C. The solution was replaced with gelation solution [monomer solution + 0.01% 4-hydroxy-TEMPO (Sigma-Aldrich, 176141), 0.2% TEMED (Bio-Rad, 1610800), 0.2% ammonium persulfate (Bio-Rad, 1610700)]. Samples were mounted between bridged glass slides (Superfrost slide with two glued 24 mm coverslips creating a gap) and incubated in a humid chamber at 37 °C for 2 h. Gelled samples were imaged prior to expansion for pre-expansion reference. Gels were then cut around each WID and digested in 8 U/ml proteinase K in digestion buffer (40 mM Tris pH 8, 1 mM EDTA, 0.5% Triton X-100, 0.8 M guanidine HCl) for 1 h at 37 °C, followed by 3 PBS washes. DNA was labeled with Hoechst 33342 (1:1000 in PBS, Invitrogen, H3570) for 1 h at room temperature, followed by 3 PBS washes. Samples were then incubated in double-distilled water for expansion, with three water exchanges prior to overnight incubation. Expanded samples were mounted in poly-L-lysine–coated μ-Slide 8 Well chambers (Ibidi, 80806), covered with water, and imaged.

Primary antibodies. rabbit polyclonal anti-pHH3 (1:200, 06-570; Millipore, for mitotic cells), anti-GFP-biotin conjugated (1:100, ab6658; Abcam, for DARE cells and clones), and anti-Fasciclin 3 (1:5, 7G10; DSHB, for cell border labeling).

Secondary antibodies. anti-rabbit Rhodamine (1:100, Jackson ImmunoResearch), Alexa Fluor® 488-Streptavidin (1:100, Jackson ImmunoResearch), and anti-mouse Atto647 (1:50, Sigma-Aldrich). Primary and secondary antibodies were incubated overnight.

Imaging and analysis. All images were acquired using an Andor Dragonfly spinning disk confocal system (Andor Technology PLC) mounted on an inverted Leica DMi8 microscope (Leica GmbH). Expansion factors were calculated by dividing the post-expansion average cell width by its pre-expansion measurement. Scale bars were adjusted by dividing by the respective expansion factor (~4×) to reflect pre-expansion dimensions.

Antibodies

Primary antibodies used in this study included rabbit polyclonal anti-cleaved human PARP (diluted 1:500, Ab2317; Abcam), rabbit polyclonal anti-pHH3 (diluted 1:300, 06-570; Millipore), and rabbit anti-cleaved Dcp-1 (diluted 1:200, 9578; Cell Signaling), anti-GFP biotin conjugated (diluted 1:100, Ab6658, Abcam), anti-Fasciclin 3 (diluted 1:5, 7G10; DSHB), Mouse Monoclonal V5 Tag Antibody (SV5-Pk1) (diluted 1:500, R960-25, Thermo Fisher Scientific). Secondary antibodies were sourced from Jackson ImmunoResearch and were used at a dilution of 1:200.

TUNEL labeling

WIDs were fixed in 4% PFA for 20 min, washed twice in PBS (2 × 5 min), washed twice (2 × 10 min) in 1xBSS (5 x BSS: 270 mM NaCl, 200 mM KCl, 37 mM MgSO4, 12 mM CaCl2.2H2O, 24 mM tricine, 1.8% glucose, and 8.5% sucrose), followed by two washes (2 × 5 min) in PBTw (0.1% Tween 20 in PBS). The samples were then refixed in 4% PFA for 20 min, washed five times (5 × 5 min) in PBTw, incubated in equilibration buffer (ApopTag kit; Millipore) for 1 h, followed by overnight incubation with the TdT enzyme in reaction buffer (ratio 3:7; ApopTag kit) at 37 °C. The reaction was stopped by replacing the reaction mix with stop buffer (diluted 1:34 in dH2O; ApopTag kit) and incubation for 3–4 h at 37 °C. The samples were then washed three times (3 × 5 min) in PBTw, blocked in BTN solution (1xBSS, 0.3% Triton X-100, and 5% normal goat serum) for 1 h at room temperature, and incubated overnight in the dark with anti-digoxigenin antibody solution (diluted 47:53 in blocking solution; ApopTag kit) at 4 °C. Samples were then washed four times (4 × 20 min) in 1xBSS, and mounted in Fluoromount-G (SouthernBiotech).

EdU incorporation assay

Dissected WIDs were immediately transferred to PBS on ice for the duration of the dissection. PBS was then replaced with EdU solution (10 μM, Click-iT™ Plus EdU Alexa Fluor™ 647 Imaging Kit; Invitrogen) prepared in standard Schneider's medium (Biological Industries), and samples were incubated for 30 min at RT. WIDs were rinsed with PBS and fixed in 4% PFA in PBS for 20 min at RT. Following fixation, samples were rinsed in 3% BSA in PBS, washed twice for 10 min each, and incubated in 0.1% Triton X-100 in PBS for 20 min at RT. Subsequent steps were carried out according to the manufacturer's protocol. All washes were performed in 3% BSA in PBS for 10 min each.

Preparation and imaging of *Drosophila* eyes

Male fly heads were detached from the bodies using a needle and then further cut to separate the two eyes. Images were captured using a stereo microscope (SZX16; Olympus) equipped with a DP28 camera (Olympus).

Quantification of imaging data

WIDs were imaged by capturing optical Z-slices at approximately 0.5-micron intervals (totaling 40 microns), resulting in about 90 Z-stacks per WID. Post-acquisition image processing and analyses were conducted using Fiji[190].

In all images except for the graphs in Fig. 9c, e, f and Fig. 10 c, quantifying the different fluorescent signals expressed in the WIDs under various genetic conditions, was done by a semi-automated ImageJ Fiji script developed to enable precise measurement of regions of interest. In brief, a 2D maximal intensity projection of the Z-stack for each imaged WID was generated. Each fluorescent channel was then thresholded and masked under careful supervision to prevent misclassification. Thresholding for the entire imaged WID was performed using a combination of all fluorescent channels. The masked images

were then used to define overlaying and divergent regions of interest for all relevant imaged channels. Measurements of the mean intensity and area of the resulting regions of interest were conducted on the corresponding original 2D maximal intensity projection images for each fluorescent channel. All regions of interest and processed images were documented and saved. The results were exported as a csv files for further statistical analysis.

For the quantifications in Fig. 9e, f and Fig. 10c images were analyzed using the open-source software Fiji[190]. For each image, 10 representative sequential slices were selected. A user-defined outline of the WID of interest was applied, and an intensity threshold was set for each dye. This enabled quantification of the areas labeled by each dye, as well as the overlap between them, on a per-slice basis. The average value across slices was then calculated for each image.

For quantification in Fig. 9c, enlarged (63× objective) images were analyzed using a dedicated pipeline in Arivis Vision4D. For each image, the average cell diameter was determined based on cell segmentation. Cells classified as 'far from DARE cells' were defined as those located at a distance greater than the average cell diameter in that image.

All analysis scripts are available on GitHub (link provided in the key resources table (Supplementary Table)).

Imaging and quantifying adult wings. Wandering 3rd instar larvae were collected at 4, 24, and 48 hpi. Adult wings were collected within one day of eclosion and imaged on a slide using a stereo microscope (MZ16F; Leica) equipped with a TOP C830 EX (TOPICA) camera and Topika Analysis software. Wing area was quantified in Fiji, with male and female wings measured separately to account for sex differences in wing size.

Data presentation, statistical analysis, and reproducibility

Illustrations in Fig. 1d, e, Fig. 2a, Fig. 3a, Fig. 5a, Fig. 6a, i, Fig. 7a, Fig. 10d, e, and Supplementary Fig. 1a, c were created using BioRender.com.

All graphs and statistical analyses in this manuscript were generated using the GraphPad Prism software version 10 for Windows (GraphPad Software, San Diego, California, USA, www.graphpad.com). The specific statistical tests used to determine significance between experimental groups, as well as details on experimental reproducibility, are provided in the relevant Fig. legends. Significance is indicated by asterisks as follows: $^{*}p < 0.05$, $^{**}p < 0.01$, $^{***}p < 0.001$, and $^{****}p < 0.0001$. All experiments were conducted with at least two biological replicates. Sample size was determined based on standard practices within the laboratory and the general field of study.

Declaration of generative AI and AI-assisted technologies in the writing process

During the preparation of this work, the author(s) used ChatGPT in order to improve the readability and language of several sentences in this work. After using this tool/service, the author(s) reviewed and edited the content as needed and take full responsibility for the content of the publication.

Reporting summary

Further information on research design is available in the Nature Portfolio Reporting Summary linked to this article.

Data availability

The authors declare that the data supporting the findings of this study are available within the paper and its supplementary information files, and that all additional data are publicly available. Source data are provided with this paper.

Code availability

The FIJI scripts used for quantifying fluorescent signals in the WID, as well as the Arivis pipeline used for quantifying proliferating cells, have been deposited in the GitHub repository[191] at https://github.com/WIS-MICC-CellObservatory/compensatory-proliferation-in-the-Drosophila-wing-.

References

1. Fuchs, Y. & Steller, H. Programmed cell death in animal development and disease. *Cell* **147**, 742–758 (2011).
2. Malin, J. Z. & Shaham, S. Cell death in C. elegans development. *Curr. Top. Dev. Biol.* **114**, 1–42 (2015).
3. Yamaguchi, Y. & Miura, M. Programmed cell death in neurodevelopment. *Dev. Cell* **32**, 478–490 (2015).
4. White, E. Mechanisms of apoptosis regulation by viral oncogenes in infection and tumorigenesis. *Cell Death. Differ.* **13**, 1371–1377 (2006).
5. Bredesen, D. E. Programmed cell death mechanisms in neurological disease. *Curr. Mol. Med.* **8**, 173–186 (2008).
6. Nagata, S., Hanayama, R. & Kawane, K. Autoimmunity and the clearance of dead cells. *Cell* **140**, 619–630 (2010).
7. Walker, N. I., Harmon, B. V., Gobe, G. C. & Kerr, J. F. Patterns of cell death. *Methods Achiev. Exp. Pathol.* **13**, 18–54 (1988).
8. Hacker, G. The morphology of apoptosis. *Cell Tissue Res* **301**, 5–17 (2000).
9. Degterev, A., Boyce, M. & Yuan, J. A decade of caspases. *Oncogene* **22**, 8543–8567 (2003).
10. Wolf, B. B. & Green, D. R. Suicidal tendencies: apoptotic cell death by caspase family proteinases. *J. Biol. Chem.* **274**, 20049–20052 (1999).
11. Budihardjo, I., Oliver, H., Lutter, M., Luo, X. & Wang, X. Biochemical pathways of caspase activation during apoptosis. *Annu Rev. Cell Dev. Biol.* **15**, 269–290 (1999).
12. Bergmann, A. The role of ubiquitylation for the control of cell death in Drosophila. *Cell Death. Differ.* **17**, 61–67 (2010).
13. Kornbluth, S. & White, K. Apoptosis in Drosophila: neither fish nor fowl (nor man, nor worm). *J. Cell Sci.* **118**, 1779–1787 (2005).
14. Salvesen, G. S. & Abrams, J. M. Caspase activation—stepping on the gas or releasing the brakes? Lessons from humans and flies. *Oncogene* **23**, 2774–2784 (2004).
15. Yuan, J., Shaham, S., Ledoux, S., Ellis, H. M. & Horvitz, H. R. The C. elegans cell death gene ced-3 encodes a protein similar to mammalian interleukin-1 beta-converting enzyme. *Cell* **75**, 641–652 (1993).
16. Bergmann, A., Agapite, J. & Steller, H. Mechanisms and control of programmed cell death in invertebrates. *Oncogene* **17**, 3215–3223 (1998).
17. Salvesen, G. S. & Riedl, S. J. Caspase mechanisms. *Adv. Exp. Med. Biol.* **615**, 13–23 (2008).
18. Riedl, S. J. & Shi, Y. Molecular mechanisms of caspase regulation during apoptosis. *Nat. Rev. Mol. Cell Biol.* **5**, 897–907 (2004).
19. Boatright, K. M. & Salvesen, G. S. Mechanisms of caspase activation. *Curr. Opin. Cell Biol.* **15**, 725–731 (2003).
20. Julien, O. & Wells, J. A. Caspases and their substrates. *Cell Death Differ.* **24**, 1380–1389 (2017).
21. Crawford, E. D. et al. Conservation of caspase substrates across metazoans suggests hierarchical importance of signaling pathways over specific targets and cleavage site motifs in apoptosis. *Cell Death. Differ.* **19**, 2040–2048 (2012).
22. Goyal, L., McCall, K., Agapite, J., Hartwieg, E. & Steller, H. Induction of apoptosis by Drosophila reaper, hid and grim through inhibition of IAP function. *EMBO J.* **19**, 589–597 (2000).
23. Vaux, D. L. & Silke, J. IAPs, RINGs and ubiquitylation. *Nat. Rev. Mol. Cell Biol.* **6**, 287–297 (2005).
24. Orme, M. & Meier, P. Inhibitor of apoptosis proteins in Drosophila: Gatekeepers of death. *Apoptosis* **14**, 950–960 (2009).
25. Bergmann, A., Yang, A. Y. P. & Srivastava, M. Regulators of IAP function: Coming to grips with the grim reaper. *Curr. Opin. Cell Biol.* **15**, 717–724 (2003).

26. Kumar, S. Caspase function in programmed cell death. *Cell Death Differ.* **14**, 32–43 (2007).
27. Cooper, D. M., Granville, D. J. & Lowenberger, C. The insect caspases. *Apoptosis* **14**, 247–256 (2009).
28. Xu, D. et al. Genetic control of programmed cell death (apoptosis) in Drosophila. *Fly* **3**, 78–90 (2009).
29. Florentin, A. & Arama, E. Caspase levels and execution efficiencies determine the apoptotic potential of the cell. *J. Cell Biol.* **196**, 513–527 (2012).
30. Xu, D., Li, Y., Arcaro, M., Lackey, M. & Bergmann, A. The CARD-carrying caspase Dronc is essential for most, but not all, developmental cell death in Drosophila. *Development* **132**, 2125–2134 (2005).
31. Srivastava, M. et al. ARK, the Apaf-1 related killer in Drosophila, requires diverse domains for its apoptotic activity. *Cell Death Differ.* **14**, 92–102 (2007).
32. Mills, K. et al. The Drosophila melanogaster Apaf-1 homologue ARK is required for most, but not all, programmed cell death. *J. Cell Biol.* **172**, 809–815 (2006).
33. Rodriguez, A. et al. Dark is a Drosophila homologue of Apaf-1/CED-4 and functions in an evolutionarily conserved death pathway. *Nat. Cell Biol.* **1**, 272–279 (1999).
34. Kanuka, H. et al. Control of the cell death pathway by Dapaf-1, a Drosophila Apaf-1/CED-4-related caspase activator. *Mol. Cell* **4**, 757–769 (1999).
35. Zhou, L., Song, Z., Tittel, J. & Steller, H. HAC-1, a Drosophila homolog of APAF-1 and CED-4, functions in developmental and radiation-induced apoptosis. *Mol. Cell* **4**, 745–755 (1999).
36. Hawkins, C. J. et al. The Drosophila caspase DRONC cleaves following glutamate or aspartate and is regulated by DIAP1, HID, and GRIM. *J. Biol. Chem.* **275**, 27084–27093 (2000).
37. Tian, L., Li, Y. & Shi, Y. Dark and Dronc activation in Drosophila melanogaster. *Proc. Natl Acad. Sci. USA* **121**, e2312784121 (2024).
38. Kamber Kaya, H. E., Ditzel, M., Meier, P. & Bergmann, A. An inhibitory mono-ubiquitylation of the Drosophila initiator caspase Dronc functions in both apoptotic and non-apoptotic pathways. *PLoS Genet.* **13**, e1006438 (2017).
39. Meier, P., Silke, J., Leevers, S. J. & Evan, G. I. The Drosophila caspase DRONC is regulated by DIAP1. *EMBO J.* **19**, 598–611 (2000).
40. Ditzel, M. et al. Inactivation of effector caspases through nondegradative polyubiquitylation. *Mol. Cell* **32**, 540–553 (2008).
41. White, K., Tahaoglu, E. & Steller, H. Cell killing by the Drosophila gene reaper. *Science* **271**, 805–807 (1996). *(1979)*.
42. Steller, H. Regulation of apoptosis in Drosophila. *Cell Death Differ.* **15**, 1132–1138 (2008).
43. Ryoo, H. D., Bergmann, A., Gonen, H., Ciechanover, A. & Steller, H. Regulation of Drosophila IAP1 degradation and apoptosis by reaper and ubcD1. *Nat. Cell Biol.* **4**, 432–438 (2002).
44. Aram, L., Yacobi-Sharon, K. & Arama, E. CDPs: Caspase-dependent non-lethal cellular processes. *Cell Death Differ.* **24**, 1307–1310 (2017).
45. Baena-Lopez, L. A. All about the caspase-dependent functions without cell death. *Semin Cell Dev. Biol.* **82**, 77–78 (2018).
46. Kuranaga, E. & Miura, M. Nonapoptotic functions of caspases: caspases as regulatory molecules for immunity and cell-fate determination. *Trends Cell Biol.* **17**, 135–144 (2007).
47. Feinstein-Rotkopf, Y. & Arama, E. Can't live without them, can live with them: roles of caspases during vital cellular processes. *Apoptosis* **14**, 980–995 (2009).
48. Yi, C. H. & Yuan, J. The Jekyll and Hyde Functions of Caspases. *Dev. Cell* **16**, 21–34 (2009).
49. Fuchs, Y. & Steller, H. Live to die another way: modes of programmed cell death and the signals emanating from dying cells. *Nat. Rev. Mol. Cell Biol.* **16**, 329–344 (2015).
50. Connolly, P. F., Jager, R. & Fearnhead, H. O. New roles for old enzymes: killer caspases as the engine of cell behavior changes. *Front Physiol.* **5**, 149 (2014).
51. Shalini, S., Dorstyn, L., Dawar, S. & Kumar, S. Old, new and emerging functions of caspases. *Cell Death Differ.* **22**, 526–539 (2015).
52. Arama, E., Baena-Lopez, L. A. & Fearnhead, H. O. Non-lethal message from the Holy Land: The first international conference on nonapoptotic roles of apoptotic proteins. *FEBS J.* **288**, 2166–2183 (2021).
53. Baena-Lopez, L. A., Arthurton, L., Xu, D. C. & Galasso, A. Non-apoptotic Caspase regulation of stem cell properties. *Semin Cell Dev. Biol.* **82**, 118–126 (2018).
54. Mollereau, B. et al. Compensatory proliferation and apoptosis-induced proliferation: a need for clarification. *Cell Death. Differ.* **20**, 181 (2013).
55. Fogarty, C. E. & Bergmann, A. Killers creating new life: Caspases drive apoptosis-induced proliferation in tissue repair and disease. *Cell Death Differ.* **24**, 1390–1400 (2017).
56. Pérez-Garijo, A. & Steller, H. Spreading the word: non-autonomous effects of apoptosis during development, regeneration and disease. *Development* **142**, 3253–3262 (2015).
57. Diwanji, N. & Bergmann, A. Two sides of the same coin—compensatory proliferation in regeneration and cancer. *Adv. Exp. Med Biol.* **1167**, 65–85 (2019).
58. Haynie, J. L. & Bryant, P. J. The effects of X-rays on the proliferation dynamics of cells in the imaginal wing disc of Drosophila melanogaster. *Wilehm Roux Arch. Dev. Biol.* **183**, 85–100 (1977).
59. Graves, B. J. & Schubiger, G. Cell cycle changes during growth and differentiation of imaginal leg discs in Drosophila melanogaster. *Dev. Biol.* **93**, 104–110 (1982).
60. Martín, F. A., Peréz-Garijo, A. & Morata, G. Apoptosis in Drosophila: compensatory proliferation and undead cells. *Int J. Dev. Biol.* **53**, 1341–1347 (2009).
61. Pérez-Garijo, A., Martín, F. A. & Morata, G. Caspase inhibition during apoptosis causes abnormal signalling and developmental aberrations in Drosophila. *Development* **131**, 5591–5598 (2004).
62. Verghese, S. & Su, T. T. Ionizing radiation induces stem cell-like properties in a caspase-dependent manner in Drosophila. *PLoS Genet.* **14**, e1007659 (2018).
63. Ryoo, H. D., Gorenc, T. & Steller, H. Apoptotic cells can induce compensatory cell proliferation through the JNK and the wingless signaling pathways. *Dev. Cell* **7**, 491–501 (2004).
64. Fan, Y. & Bergmann, A. Distinct mechanisms of apoptosis-induced compensatory proliferation in proliferating and differentiating tissues in the Drosophila eye. *Dev. Cell* **14**, 399–410 (2008).
65. Huh, J. R., Guo, M. & Hay, B. A. Compensatory proliferation induced by cell death in the Drosophila wing disc requires activity of the apical cell death caspase dronc in a nonapoptotic role. *Curr. Biol.* **14**, 1262–1266 (2004).
66. Ryoo, H. D. & Bergmann, A. The role of apoptosis-induced proliferation for regeneration and cancer. *Cold Spring Harb. Perspect. Biol.* **4**, a008797 (2012).
67. Kashio, S., Obata, F. & Miura, M. Interplay of cell proliferation and cell death in Drosophila tissue regeneration. *Dev. Growth Differ.* **56**, 368–375 (2014).
68. Amcheslavsky, A., Lindblad, J. L. & Bergmann, A. Transiently 'Undead' Enterocytes Mediate Homeostatic Tissue Turnover in the Adult Drosophila Midgut. *Cell Rep.* **33**, 108408 (2020).
69. Amcheslavsky, A. et al. Plasma membrane localization of apoptotic caspases for non-apoptotic functions. *Dev. Cell* **45**, 450–464.e3 (2018).
70. Farrell, L. et al. Actin remodeling mediates ROS production and JNK activation to drive apoptosis-induced proliferation. *PLoS Genet* **18**, e1010533 (2022).

71. Fan, Y. & Bergmann, A. Apoptosis-induced compensatory proliferation. The Cell is dead. Long live the Cell! *Trends Cell Biol.* **18**, 467–473 (2008).
72. Domingos, P. M. & Steller, H. Pathways regulating apoptosis during patterning and development. *Curr. Opin. Genet Dev.* **17**, 294–299 (2007).
73. Pérez-Garijo, A., Shlevkov, E. & Morata, G. The role of Dpp and Wg in compensatory proliferation and in the formation of hyperplastic overgrowths caused by apoptotic cells in the Drosophila wing disc. *Development* **136**, 1169–1177 (2009).
74. Orme, M. H. et al. The unconventional myosin CRINKLED and its mammalian orthologue MYO7A regulate caspases in their signalling roles. *Nat Commun* **7**, (2016).
75. Gorelick-Ashkenazi, A. et al. Caspases maintain tissue integrity by an apoptosis-independent inhibition of cell migration and invasion. *Nat. Commun.* **9**, 2806 (2018).
76. Wells, B. S., Yoshida, E. & Johnston, L. A. Compensatory proliferation in Drosophila imaginal discs requires Dronc-dependent p53 activity. *Curr. Biol.* **16**, 1606–1615 (2006).
77. Kondo, S., Senoo-Matsuda, N., Hiromi, Y. & Miura, M. DRONC coordinates cell death and compensatory proliferation. *Mol. Cell Biol.* **26**, 7258–7268 (2006).
78. Gulyas, L., Lari, A., Shah, S. B. & Glaunsinger, B. A. Cleavage of the RNA polymerase II general transcription factor TFIIB tunes transcription during stress. *bioRxiv*, https://doi.org/10.1101/2025.07.28.667251 (2025).
79. Gulyas, L. & Glaunsinger, B. A. RNA polymerase II subunit modulation during viral infection and cellular stress. *Curr. Opin. Virol.* **56**, 101259 (2022).
80. Trivigno, D., Bornes, L., Huber, S. M. & Rudner, J. Regulation of protein translation initiation in response to ionizing radiation. *Radiat. Oncol.* **8**, 1–12 (2013).
81. Holcik, M., Sonenberg, N. & Korneluk, R. G. Internal ribosome initiation of translation and the control of cell death. *Trends Genet.* **16**, 469–473 (2000).
82. Sheikh, M. S. & Fornace, A. J. Regulation of translation initiation following stress. *Oncogene* **18**, 6121–6128 (1999). *1999 18:45*.
83. Bresson, S. et al. Stress-induced translation inhibition through rapid displacement of scanning initiation factors. *Mol. Cell* **80**, 470 (2020).
84. Baena-Lopez, L. A. et al. Novel initiator caspase reporters uncover previously unknown features of caspase-activating cells. *Development* **145**, dev170811 (2018).
85. Mollereau, B. & Domingos, P. M. Photoreceptor differentiation in Drosophila: from immature neurons to functional photoreceptors. *Dev. Dyn.* **232**, 585–592 (2005).
86. Evans, C. J. et al. G-TRACE: rapid Gal4-based cell lineage analysis in Drosophila. *Nat. Methods* **6**, 603–605 (2009).
87. Kiger, J., Natzle, J. E. & Green, M. M. Hemocytes are essential for wing maturation in Drosophila melanogaster. *Proc. Natl Acad. Sci. USA* **98**, 10190–10195 (2001).
88. Kiger, J. A. et al. Tissue remodeling during maturation of the Drosophila wing. *Dev. Biol.* **301**, 178–191 (2007).
89. Link, N. et al. A collective form of cell death requires homeodomain interacting protein kinase. *J. Cell Biol.* **178**, 567–574 (2007).
90. Garcia-Hughes, G., Link, N., Ghosh, A. B. & Abrams, J. M. Hid arbitrates collective cell death in the Drosophila wing. *Mech. Dev.* **138**, 349–355 (2015).
91. Wilson, R. et al. The DIAP1 RING finger mediates ubiquitination of Dronc and is indispensable for regulating apoptosis. *Nat. Cell Biol.* **4**, 445–450 (2002).
92. Hay, B. A., Wolff, T. & Rubin, G. M. Expression of baculovirus P35 prevents cell death in Drosophila. *Development* **120**, 2121–2129 (1994).
93. Bump, N. J. et al. Inhibition of ICE family proteases by baculovirus antiapoptotic protein p35. *Science* **269**, 1885–1888 (1995).
94. Lannan, E., Vandergaast, R. & Friesen, P. D. Baculovirus caspase inhibitors P49 and P35 block virus-induced apoptosis downstream of effector caspase DrICE activation in Drosophila melanogaster cells. *J. Virol.* **81**, 9319–9330 (2007).
95. Zimmermann, K. C., Ricci, J. E., Droin, N. M. & Green, D. R. The role of ARK in stress-induced apoptosis in Drosophila cells. *J. Cell Biol.* **156**, 1077–1087 (2002).
96. Coutelis, J., González-Morales, N., Géminard, C. & Noselli, S. Diversity and convergence in the mechanisms establishing L/R asymmetry in metazoa. *EMBO Rep.* **15**, 926–937 (2014).
97. Halpern, M. E., Hobert, O. & Wright, C. V. E. Left-right asymmetry: advances and enigmas. *Genesis* **52**, 451–454 (2014).
98. Géminard, C., González-Morales, N., Coutelis, J. B. & Noselli, S. The myosin ID pathway and left-right asymmetry in Drosophila. *Genesis* **52**, 471–480 (2014).
99. Kang, Y., Neuman, S. D. & Bashirullah, A. Tango7 regulates cortical activity of caspases during reaper-triggered changes in tissue elasticity. *Nat Commun.* **8**, 603 (2017).
100. Fan, Y. et al. Genetic models of apoptosis-induced proliferation decipher activation of JNK and identify a requirement of EGFR signaling for tissue regenerative responses in Drosophila. *PLoS Genet* **10**, e1004131 (2014).
101. Bergantiños, C., Corominas, M. & Serras, F. Cell death-induced regeneration in wing imaginal discs requires JNK signalling. *Development* **137**, 1169–1179 (2010).
102. Herrera, S. C., Martín, R. & Morata, G. Tissue homeostasis in the wing disc of Drosophila melanogaster: immediate response to massive damage during development. *PLoS Genet.* **9**, e1003446 (2013).
103. Fogarty, C. E. et al. Extracellular reactive oxygen species drive apoptosis-induced proliferation via Drosophila macrophages. *Curr. Biol.* **26**, 575–584 (2016).
104. Xu, D. C., Wang, L., Yamada, K. M. & Baena-Lopez, L. A. Non-apoptotic activation of Drosophila caspase-2/9 modulates JNK signaling, the tumor microenvironment, and growth of wound-like tumors. *Cell Rep.* **39**, 110718 (2022).
105. Wada, Y., Ohsawa, S. & Igaki, T. Yorkie ensures robust tissue growth in Drosophila ribosomal protein mutants. *Development* **148**, 198705 (2021).
106. Ichijo, H. et al. Induction of apoptosis by ASK1, a mammalian MAPKKK that activates SAPK/JNK and p38 signaling pathways. *Science* **275**, 90–94 (1997).
107. Tobiume, K. et al. ASK1 is required for sustained activations of JNK/p38 MAP kinases and apoptosis. *EMBO Rep.* **2**, 222–228 (2001).
108. Harper, S. J. & Lograsso, P. Signalling for survival and death in neurones: The role of stress-activated kinases, JNK and p38. *Cell Signal* **13**, 299–310 (2001).
109. Johnson, G. L. & Lapadat, R. Mitogen-activated protein kinase pathways mediated by ERK, JNK, and p38 protein kinases. *Science* **298**, 1911–1912 (2002).
110. Wagner, E. F. & Nebreda, ÁR. Signal integration by JNK and p38 MAPK pathways in cancer development. *Nat. Rev. Cancer* **9**, 537–549 (2009).
111. Patel, P. H. et al. Damage sensing by a Nox-Ask1-MKK3-p38 signaling pathway mediates regeneration in the adult Drosophila midgut. *Nat Commun.* **10**, 4365 (2019).
112. Santabárbara-Ruiz, P. et al. Ask1 and Akt act synergistically to promote ROS-dependent regeneration in Drosophila. *PLoS Genet* **15**, e1007926 (2019).
113. Esteban-Collado, J., Corominas, M. & Serras, F. Nutrition and PI3K/Akt signaling are required for p38-dependent regeneration. *Development* **148**, 197087 (2021).

114. Esteban-Collado, J. et al. Reactive oxygen species activate the Drosophila TNF receptor Wengen for damage-induced regeneration. *EMBO J.* **43**, 3604–3626 (2024).
115. McEwen, D. G. & Peifer, M. Puckered, a Drosophila MAPK phosphatase, ensures cell viability by antagonizing JNK-induced apoptosis. *Development* **132**, 3935–3946 (2005).
116. Karkali, K. & Panayotou, G. The Drosophila DUSP Puckered is phosphorylated by JNK and p38 in response to arsenite-induced oxidative stress. *Biochem. Biophys. Res. Commun.* **418**, 301–306 (2012).
117. Belozerov, V. E., Lin, Z.-Y., Gingras, A.-C., McDermott, J. C. & Michael Siu, K. W. High-Resolution protein interaction Map of the Drosophila melanogaster p38 mitogen-activated protein kinases reveals limited functional redundancy. *Mol. Cell Biol.* **32**, 3695 (2012).
118. Chen, J. et al. Participation of the p38 pathway in Drosophila host defense against pathogenic bacteria and fungi. *Proc. Natl Acad. Sci. USA* **107**, 20774–20779 (2010).
119. Martín-Blanco, E. et al. puckered encodes a phosphatase that mediates a feedback loop regulating JNK activity during dorsal closure in Drosophila. *Genes Dev.* **12**, 557–670 (1998).
120. Chatterjee, N. & Bohmann, D. A versatile φC31 based reporter system for measuring AP-1 and NRF2 signaling in Drosophila and in tissue culture. *PLoS One* **7**, e34063 (2012).
121. Humar, M. et al. The mitogen-activated protein kinase p38 regulates activator protein 1 by direct phosphorylation of c-Jun. *Int. J. Biochem. Cell Biol.* **39**, 2278–2288 (2007).
122. Tanos, T. et al. Phosphorylation of c-Fos by members of the p38 MAPK family: Role in the AP-1 response to UV light. *J. Biol. Chem.* **280**, 18842–18852 (2005).
123. Hazzalin, C. A., Cuenda, A., Cano, E., Cohen, P. & Mahadevan, L. C. Effects of the inhibition of p38/RK MAP kinase on induction of five fos and jun genes by diverse stimuli. *Oncogene* **15**, 2321–2331 (1997).
124. Dichtel-Danjoy, M. L. et al. Drosophila p53 isoforms differentially regulate apoptosis and apoptosis-induced proliferation. *Cell Death Differ.* **20**, 108–116 (2013).
125. Shlevkov, E. & Morata, G. A dp53/JNK-dependant feedback amplification loop is essential for the apoptotic response to stress in Drosophila. *Cell Death Differ.* **19**, 451 (2011).
126. Palmerini, V. et al. Drosophila TNFRs Grindelwald and Wengen bind Eiger with different affinities and promote distinct cellular functions. *Nat. Commun.* **12**, 1–12 (2021). *2021 12:1*.
127. Zhang, P. et al. Inter-cell type interactions that control JNK signaling in the Drosophila intestine. *Nat. Commun.* **15**, 1–14 (2024).
128. Kanda, H., Igaki, T., Kanuka, H., Yagi, T. & Miura, M. Wengen, a member of the Drosophila tumor necrosis factor receptor superfamily, is required for Eiger signaling. *J. Biol. Chem.* **277**, 28372–28375 (2002).
129. Kauppila, S. et al. Eiger and its receptor, Wengen, comprise a TNF-like system in Drosophila. *Oncogene* **22**, 4860–4867 (2003).
130. Andersen, D. S. et al. The Drosophila TNF receptor Grindelwald couples loss of cell polarity and neoplastic growth. *Nature* **522**, 482–486 (2015).
131. Soares, C. C., Rizzo, A., Maresma, M. F. & Meier, P. Autocrine glutamate signaling drives cell competition in Drosophila. *Dev. Cell* https://doi.org/10.1016/J.DEVCEL.2024.06.022 (2024)
132. Yu, L., Hébert, M. C. & Zhang, Y. E. TGF-β receptor-activated p38 MAP kinase mediates Smad-independent TGF-β responses. *EMBO J.* **21**, 3749 (2002).
133. Gong, K. et al. A novel protein kinase A-independent, β-Arrestin-1-dependent signaling pathway for p38 mitogen-activated protein kinase activation by β2-adrenergic receptors. *J. Biol. Chem.* **283**, 29028 (2008).
134. Zarubin, T. & Han, J. Activation and signaling of the p38 MAP kinase pathway. *Cell Res.* **15**, 11–18 (2005).
135. Adachi-Yamada, T. et al. p38 mitogen-activated protein kinase can be involved in transforming growth factor β superfamily signal transduction in Drosophila wing morphogenesis. *Mol. Cell Biol.* **19**, 2322 (1999).
136. Schnyder-Candrian, S. et al. Dual effects of p38 MAPK on TNF-dependent bronchoconstriction and tnf-independent neutrophil recruitment in lipopolysaccharide-induced acute respiratory distress syndrome. *J. Immunol.* **175**, 262–269 (2005).
137. Jurado-Pueyo, M., Campos, P. M., Mayor, F. & Murga, C. GRK2-dependent desensitization downstream of G proteins. *J. Recept. Signal. Transduct.* **28**, 59–70 (2008).
138. Igaki, T. et al. Eiger, a TNF superfamily ligand that triggers the Drosophila JNK pathway. *EMBO J.* **21**, 3009–3018 (2002).
139. Diwanji, N. & Bergmann, A. Basement membrane damage by ROS- and JNK-mediated Mmp2 activation drives macrophage recruitment to overgrown tissue. *Nat. Commun.* **11**, 1–14 (2020). *2020 11:1*.
140. Stephenson, H. N., Streeck, R., Grüblinger, F., Goosmann, C. & Herzig, A. Hemocytes are essential for Drosophila melanogaster post-embryonic development, independent of control of the microbiota. *Development* **149**, dev200286 (2022).
141. Lane, M. E. et al. Dacapo, a cyclin-dependent kinase inhibitor, stops cell proliferation during Drosophila development. *Cell* **87**, 1225–1235 (1996).
142. De Nooij, J. C., Letendre, M. A. & Hariharan, I. K. A cyclin-dependent kinase inhibitor, dacapo, is necessary for timely exit from the cell cycle during Drosophila Embryogenesis. *Cell* **87**, 1237–1247 (1996).
143. Strahl, B. D. & Allis, C. D. The language of covalent histone modifications. *Nature* **403**, 41–45 (2000).
144. Pérez, E., Lindblad, J. L. & Bergmann, A. Tumor-promoting function of apoptotic caspases by an amplification loop involving ROS, macrophages and JNK in Drosophila. *Elife* **6**, e26747 (2017).
145. Pinal, N., Calleja, M. & Morata, G. Pro-apoptotic and pro-proliferation functions of the JNK pathway of Drosophila: roles in cell competition, tumorigenesis and regeneration. *Open Biol.* **9**, 180256 (2019).
146. D'Brot, A. et al. Tango7 directs cellular remodeling by the Drosophila apoptosome. *Genes Dev.* **27**, 1650–1655 (2013).
147. Chew, S. K. et al. Genome-wide silencing in Drosophila captures conserved apoptotic effectors. *Nature* **460**, 123–127 (2009).
148. Ko, Y. S. et al. MYO1D binds with kinase domain of the EGFR family to anchor them to plasma membrane before their activation and contributes carcinogenesis. *Oncogene* **38**, 7416–7432 (2019).
149. Ko, Y.-S. et al. New strategy for suppressing the growth of lung cancer cells harboring mutations in the ATP-binding region of EGFR by targeting the molecular motor MYO1D. *Clin. Transl. Med* **11**, e515 (2021).
150. Suissa, Y., Ziv, O., Dinur, T., Arama, E. & Gerlitz, O. The NAB-Brk signal bifurcates at JNK to independently induce apoptosis and compensatory proliferation. *J. Biol. Chem.* **286**, 15556–15564 (2011).
151. Warner, S. J., Yashiro, H. & Longmore, G. D. The Cdc42/Par6/aPKC polarity complex regulates apoptosis-induced compensatory proliferation in epithelia. *Curr. Biol.* **20**, 677–686 (2010).
152. Liu, J. & Lin, A. Role of JNK activation in apoptosis: a double-edged sword. *Cell Res.* **15**, 36–42 (2005).
153. Bogoyevitch, M. A. & Kobe, B. Uses for JNK: the many and varied substrates of the c-Jun N-terminal kinases. *Microbiol. Mol. Biol. Rev.* **70**, 1061–1095 (2006).
154. Zeke, A., Misheva, M., Reményi, A. & Bogoyevitch, M. A. JNK signaling: regulation and functions based on complex protein-protein partnerships. *Microbiol. Mol. Biol. Rev.* **80**, 793–835 (2016).

155. La Marca, J. E. & Richardson, H. E. Two-Faced: Roles of JNK signalling during tumourigenesis in the Drosophila model. *Front Cell Dev. Biol.* **8**, 42 (2020).
156. Shlevkov, E. & Morata, G. A dp53/JNK-dependant feedback amplification loop is essential for the apoptotic response to stress in Drosophila. *Cell Death Differ.* **19**, 451–460 (2012).
157. Kuranaga, E. et al. Reaper-mediated inhibition of DIAP1-induced DTRAF1 degradation results in activation of JNK in Drosophila. *Nat. Cell Biol.* **4**, 705–710 (2002).
158. Dominici, S. et al. Endogenous oxidative stress induces distinct redox forms of tumor necrosis factor receptor-1 in melanoma cells. *Ann. N. Y Acad. Sci.* **1030**, 62–68 (2004).
159. Ozsoy, H. Z., Sivasubramanian, N., Wieder, E. D., Pedersen, S. & Mann, D. L. Oxidative stress promotes ligand-independent and enhanced ligand-dependent tumor necrosis factor receptor signaling. *J. Biol. Chem.* **283**, 23419–23428 (2008).
160. Verghese, S. & Su, T. T. Drosophila Wnt and STAT define apoptosis-resistant epithelial cells for tissue regeneration after irradiation. *PLoS Biol.* **14**, e1002536 (2016).
161. Sun, G., Ding, X. A., Argaw, Y., Guo, X. & Montell, D. J. Akt1 and dCIZ1 promote cell survival from apoptotic caspase activation during regeneration and oncogenic overgrowth. *Nat. Commun.* **11**, 1–16 (2020). *2020 11:1*.
162. Colon Plaza, S. & Su, T. T. Ionizing radiation induces cells with past caspase activity that contribute to the adult organ in Drosophila and show reduced Loss of Heterozygosity. *Cell Death Discov.* **10**, 6 (2024).
163. Tang, H. L., Tang, H. M., Fung, M. C. & Hardwick, J. M. In vivo CaspaseTracker biosensor system for detecting anastasis and non-apoptotic caspase activity. *Sci. Rep.* **5**, 9015 (2015).
164. Ding, A. X. et al. CasExpress reveals widespread and diverse patterns of cell survival of caspase-3 activation during development in vivo. *Elife* **5**, e10936 (2016).
165. Wells, B. S. & Johnston, L. A. Maintenance of imaginal disc plasticity and regenerative potential in Drosophila by p53. *Dev. Biol.* **361**, 263–276 (2012).
166. Hanahan, D. & Weinberg, R. A. Hallmarks of cancer: The next generation. *Cell* **144**, 646–674 (2011).
167. Fernandez, L. P. et al. Pigmentation-related genes and their implication in malignant melanoma susceptibility. *Exp. Dermatol* **18**, 634–642 (2009).
168. Tournier, C. The 2 faces of JNK signaling in cancer. *Genes Cancer* **4**, 397 (2013).
169. Wu, Q. et al. JNK signaling in cancer cell survival. *Med Res Rev.* **39**, 2082–2104 (2019).
170. Hammouda, M. B., Ford, A. E., Liu, Y. & Zhang, J. Y. The JNK signaling pathway in inflammatory skin disorders and cancer. *Cells* **9**, 857 (2020).
171. Lee, E. H. et al. Role of the JNK pathway in bladder cancer. *Onco Targets Ther.* **15**, 963–971 (2022).
172. Igaki, T., Pagliarini, R. A. & Xu, T. Loss of cell polarity drives tumor growth and invasion through JNK activation in Drosophila. *Curr. Biol.* **16**, 1139–1146 (2006).
173. Enomoto, M., Kizawa, D., Ohsawa, S. & Igaki, T. JNK signaling is converted from anti- to pro-tumor pathway by Ras-mediated switch of Warts activity. *Dev. Biol.* **403**, 162–171 (2015).
174. Ma, X. et al. PP6 disruption synergizes with oncogenic Ras to promote JNK-dependent tumor growth and invasion. *Cell Rep.* **19**, 2657–2664 (2017).
175. Cong, B. et al. JNK and Yorkie drive tumor malignancy by inducing L-amino acid transporter 1 in Drosophila. *PLoS Genet* **17**, e1009893 (2021).
176. Los, M. et al. Anticancer drugs of tomorrow: apoptotic pathways as targets for drug design. *Drug Discov. Today* **8**, 67–77 (2003).
177. Lim, B., Greer, Y., Lipkowitz, S. & Takebe, N. Novel apoptosis-inducing agents for the treatment of cancer, a new arsenal in the toolbox. *Cancers* **11**, 1087 (2019).
178. Carneiro, B. A. & El-Deiry, W. S. Targeting apoptosis in cancer therapy. *Nat. Rev. Clin. Oncol.* **17**, 395–417 (2020).
179. Hickman, J. A. Apoptosis induced by anticancer drugs. *Cancer Metastasis Rev.* **11**, 121–139 (1992).
180. Kaufmann, S. H. & Earnshaw, W. C. Induction of apoptosis by cancer chemotherapy. *Exp. Cell Res* **256**, 42–49 (2000).
181. Furdui, C. M. Ionizing radiation: mechanisms and therapeutics. *Antioxid. Redox Signal* **21**, 218 (2014).
182. Sia, J., Szmyd, R., Hau, E. & Gee, H. E. Molecular mechanisms of radiation-induced cancer cell death: a primer. *Front .Cell Dev. Biol.* **8**, 512111 (2020).
183. Mirzaie-Joniani, H. et al. Apoptosis induced by low-dose and low-dose-rate radiation. *Cancer* **94**, 1210–1214 (2002).
184. Cao, X. et al. Radiation induces apoptosis primarily through the intrinsic pathway in mammalian cells. *Cell Signal* **62**, 109337 (2019).
185. Vilalta, M., Rafat, M. & Graves, E. E. Effects of radiation on metastasis and tumor cell migration. *Cell. Mol. Life Sci.* **73**, 2999–3007 (2016).
186. Delaney, G., Jacob, S., Featherstone, C. & Barton, M. The role of radiotherapy in cancer treatment. *Cancer* **104**, 1129–1137 (2005).
187. Chen, H. H. W. & Kuo, M. T. Improving radiotherapy in cancer treatment: promises and challenges. *Oncotarget* **8**, 62742 (2017).
188. Kyaw, J. Y. A. et al. Systematic review and meta-analysis of the association between radiation therapy treatment volume and patient outcomes. *Int. J. Radiat. Oncol.*Biol.*Phys.* **117**, 1063–1086 (2023).
189. Jiang, N. et al. Superresolution imaging of Drosophila tissues using expansion microscopy. *Mol. Biol. Cell* **29**, 1413–1421 (2018).
190. Schindelin, J. et al. Fiji: An open-source platform for biological-image analysis. *Nat. Methods* **9**, 676–682 (2012).
191. Braun, T. et al. Apoptosis-resistant cells drive compensatory proliferation via cell-autonomous and non-autonomous functions of the initiator caspase Dronc. *GitHub*, https://doi.org/10.5281/zenodo.17356314, (2025)

Acknowledgements

We thank Pascal Meier, Masayuki Miura, Oren Schuldiner, François Schweisguth, Talila Volk, the Vienna *Drosophila* Resource Center (VDRC), the Transgenic RNAi Project (TRiP), and the Bloomington *Drosophila* Stock Center for providing essential stocks and reagents. We also appreciate Ron Rotkopf for his assistance with statistical analysis, Anna Gorelick-Ashkenazi for providing the control image for the *CPV* reporter, and the Arama laboratory members for their encouragement and advice. Additionally, we acknowledge the BioRender website for its role in creating the illustrations used in this paper. This research was supported by a grant from the Israel Science Foundation (grant No. 1378/24) and a grant from the European Research Council under the EU's Seventh Framework Program (FP/2007-2013)/ERC grant agreement (616088). E.A. also receives internal research support from the Weizmann Institute of Science, including funding from the Kekst Family Institute for Medical Genetics, the Crown Human Genome Center, and the estate of Betty Weneser. E.A. holds the Harry Kay Professional Chair of Cancer Research. L.A. B.-L. was supported by a Spanish Government grant PID2023-150773NB-I00 (MCIN/AEI/10.13039/501100011033). A.B. is funded by the National Institute of General Medical Sciences (NIGMS) R35GM118330. A.B. notes that the content is solely the responsibility of the authors and does not necessarily represent the official views of the NIH.

Author contributions

T.B. designed, performed, and analyzed the experiments and conducted statistical analyses. N.A. provided technical assistance for specific experiments. L.S. developed the data analysis code used to quantify most experiments (except those shown in Figs. 9c, e, f, and 10c). She also generated the *actDrice* construct (Supplementary Fig. 1c) and performed the experiments in Supplementary Fig. 1d, e. E.S. developed the data analysis code for the EdU assay and double-irradiation experiments, and established the pipeline for assessing the proximity of proliferating NARE cells to DARE cells (Fig. 9c). A.B. provided valuable advice and reagents throughout the project. L.A.B.-L. provided the $_{R}$*DBS* and $_{D}$*DBS* genetic reporters prior to their publication, along with additional reagents and valuable advice. K.Y.-S. performed the expansion microscopy experiments and imaging, and provided guidance during the early stages of the study. E.A. conceived and led the project, designed experiments, interpreted results, supervised the study, wrote the manuscript, and secured funding.

Competing interests

The authors declare no competing interests.

Additional information

Supplementary information The online version contains supplementary material available at https://doi.org/10.1038/s41467-025-65996-2.

Correspondence and requests for materials should be addressed to Eli Arama.

Peer review information *Nature Communications* thanks the anonymous reviewers for their contribution to the peer review of this work. A peer review file is available.